

# Generalized promotion time cure model: A new modeling framework to identify cell-type-specific genes and improve survival prognosis

Zhi Zhao<sup>1</sup>, Fatih Kizilaslan<sup>1</sup>, Shixiong Wang<sup>2</sup>, and Manuela Zucknick<sup>1,3</sup>

<sup>1</sup>Oslo Centre for Biostatistics and Epidemiology (OCBE), University of Oslo, Norway

<sup>2</sup>Department of Clinical Molecular Biology(EpiGen), Akershus University Hospital, Norway

<sup>3</sup>Oslo Centre for Biostatistics and Epidemiology (OCBE), Oslo University Hospital, Norway

## Abstract

Single-cell technologies provide an unprecedented opportunity for dissecting the interplay between the cancer cells and the associated tumor microenvironment, and the produced high-dimensional omics data should also augment existing survival modeling approaches for identifying tumor cell type-specific genes predictive of cancer patient survival. However, there is no statistical model to integrate multiscale data including individual-level survival data, multicellular-level cell composition data and cellular-level single-cell omics covariates. We propose a class of Bayesian generalized promotion time cure models (GPTCMs) for the multiscale data integration to identify cell-type-specific genes and improve cancer prognosis. We demonstrate with simulations in both low- and high-dimensional settings that the proposed Bayesian GPTCMs are able to identify cell-type-associated covariates and improve survival prediction.

**Keywords:** Intra-tumor heterogeneity, cellular population, progression-free survival, multiscale data integration, Bayesian hierarchical modeling, variable selection

## 1 Introduction

Accurate disease risk prediction based on genomic and clinical data can lead to more effective disease screening, early prevention, and personalized treatment strategies. However, despite the identifications of hundreds of disease-associated genomic and molecular features for many disease traits through genome-wide studies in the past two decades, drug resistance often causes the targeted therapies to fail in cancer patients, which is largely due to tumor heterogeneity (Zhang et al., 2022). For advanced cancers, tumor heterogeneity encompasses both the malignant cells and their microenvironment, which makes it challenging to develop accurate prediction models for personalized treatment strategies that account for intratumor heterogeneity.

Single-cell technologies provide an unprecedented opportunity for dissecting the interplay between the cancer cells and the associated tumor microenvironment (TME), and the produced high-dimensional omics data should also augment existing survival modeling approaches for identifying tumor cell type-specific genes predictive of cancer patient survival. Current literature and contemporary insights from cancer biology reveal that deciphering the composition of the TME is critical for understanding tumorigenesis, prognosis

and responsiveness to immunotherapies (Cai et al., 2024), but current computational approaches often map the findings from single-cell omics features to large-scale bulk sequencing omics features and then jointly analyzing the bulk omics and survival data, rather than directly modeling single-cell omics and survival data (Zhao et al., 2024b). Although there are multiple survival models (Yakovlev et al., 1996; Chen et al., 1999; Cooner et al., 2007; Kim et al., 2011; Gómez et al., 2023) motivated by the growth of clonogenic tumor cells, they cannot jointly model individual-level survival data and (multi-)cellular-level omics data.

Our previous work Zhao and Kızılaslan (2024) provides a new modeling framework, generalized promotion time cure model (GPTCM), for multiscale data integration including individual-level survival data, multicellular-level cell composition data and cellular-level single-cell omics covariates. In this article, we develop a class of Bayesian versions of GPTCM to identify cell-type-specific genes and improve survival prognosis. We also present complete statistical inference for the proposed Bayesian GPTCMs, and investigate the model performance through systematic simulations in both low- and high-dimensional settings.

The rest of the article is organized as follows. In Section 2, we propose six Bayesian versions of GPTCM and present Bayesian inference for the estimation of the proposed models. In Section 3, we compare the performances of the proposed Bayesian GPTCMs and classical survival models through simulation in low- and high-dimensional settings. In Section 4, we conclude the article with a discussion.

## 2 Generalized promotion time cure model

### 2.1 Framework of GPTCM

The generalized promotion time cure model (GPTCM) (Zhao and Kızılaslan, 2024) was motivated by the classical promotion time cure model (PTCM) (Yakovlev et al., 1996). Instead of assuming all clonogenic tumor cells homogeneous in PTCM, the generalized model version, GPTCM, assumes that the clonogenic tumor cells are a composition of multiple tumor cell subtypes in order to capture intra-tumor heterogeneity for better modeling tumor evolution and for better predicting cancer patient survival. Suppose that a patient after an initial treatment has the total count of tumor cells  $N = \sum_{l=1}^L N_l$ ,  $L \geq 2$ , where  $N_l$  is the number of cells in the  $l$ -th tumor cell subtype, and suppose the total count  $N \sim \text{Poisson}(\theta)$  with  $\theta > 0$ . Given the total count  $N$ , the counts of individual tumor cell subtypes follow a multinomial distribution, i.e.  $(N_1, \dots, N_L) \sim \text{Mult}(\mathbf{p}_1, \dots, \mathbf{p}_L)$ , where the sum of the  $L$  probabilities is  $\sum_{l=1}^L \mathbf{p}_l = 1$ . To generalize the PTCM, suppose the  $l$ -th cell type has multivariate random times for its  $N_l$  clonogenic tumor cells propagating into a newly detectable tumor:

$$\mathbf{W}_l = \left( Z_{\sum_{j=1}^{l-1} N_{j-1} + 1}, \dots, Z_{\sum_{j=1}^{l-1} N_{j-1} + N_l} \right),$$

where  $Z_{\bullet}$  is the random time for a clonogenic cell to produce a detectable tumor mass,  $l \in \{1, \dots, L\}$ ,  $N_0 = 0$ . For the  $N_l$  homogeneous cells in the  $l$ -th cell type, we assume a cell-type-specific promotion time distribution  $F_l(t) = 1 - S_l(t)$ ,  $l \in \{1, \dots, L\}$ . The time to tumor recurrence can be defined as  $T = \min\{\min\{\mathbf{W}_1\}, \dots, \min\{\mathbf{W}_L\}\}$ , i.e. the time when the first clonogenic cell in one cell type becomes activated.

Then Zhao and Kızılaslan (2024) derived the population survival function as

$$\begin{aligned}
S_{pop}(t) &= \mathbb{P}(\text{no cancer by time } t) \\
&= \mathbb{P}(N = 0) + \mathbb{P}(\min\{\min\{\mathbf{W}_1\}, \dots, \min\{\mathbf{W}_L\}\} > t, N > 0) \\
&= e^{-\theta\{1 - \sum_{l=1}^L p_l S_l(t)\}}.
\end{aligned} \tag{1}$$

If the promotion time distributions of different cell types are the same, i.e.  $S(t) = S_l(t)$ ,  $\forall l \in \{1, \dots, L\}$ , the population survival function (1) is degenerated into PTCM (Yakovlev et al., 1996), i.e.  $S_{pop}(t) = e^{-\theta\{1 - S(t)\}}$ . Note that the population survival function will not become zero when the time tends to infinity, i.e. some patients will never encounter the event of interest. Patients who will never encounter the event of interest belong to the cured population (with a fraction  $e^{-\theta}$ ), and patients who will potentially encounter the event of interest always after a finite time point belong to the noncured population.

In both PTCM and GPTCM, covariates can be introduced into the Poisson rate parameter  $\theta$  through a log-linear submodel:

$$\log \theta = \xi_0 + \mathbf{X}_0 \boldsymbol{\xi}, \tag{2}$$

where  $\mathbf{X}_0 \in \mathbb{R}^{n \times d}$  is a data matrix of  $d$  mandatory variables from  $n$  subjects, and coefficients  $\boldsymbol{\xi} = (\xi_1, \dots, \xi_d)^\top$ . As indicated in Zhao and Kızılaslan (2024), benefiting from the mixture part  $\sum_{l=1}^L p_l S_l(t)$  in GPTCM (1), cell-type-specific covariates (e.g. genetic variables from each tumor cell subtype)  $\mathbf{X}_l \in \mathbb{R}^{n \times p}$  can be introduced into the survival function  $S_l(t)$ . For example, we can model a Weibull's mean parameter  $\boldsymbol{\mu}_l \in \mathbb{R}^n$  by cell-type-specific covariates  $\mathbf{X}_l$ :

$$\begin{aligned}
S_l(t) &= \exp\{-(t/\boldsymbol{\lambda}_l)^\kappa\}, \\
\boldsymbol{\lambda}_l &= \frac{\boldsymbol{\mu}_l}{\Gamma(1 + 1/\kappa)}, \\
\log \boldsymbol{\mu}_l &= \beta_{0l} + \mathbf{X}_l \boldsymbol{\beta}_l,
\end{aligned}$$

where  $\kappa \in \mathbb{R}_+$  is the Weibull's shape parameter and  $\Gamma(\cdot)$  is the gamma function.

We will propose six Bayesian versions of GPTCM as shown in Table 1 suited for modeling low- and high-dimensional covariates, and present full Bayesian inference for the six models. For the simplicity of notations, we assume the same number of covariates from different cell types, i.e.  $\mathbf{X}_1, \dots, \mathbf{X}_L$  have the same number of columns. However, the proposed models can deal with different numbers of covariates from different cell types.

Table 1: Bayesian GPTCMs

	GPTCM-noBVS1	GPTCM-noBVS2	GPTCM-Ber1	GPTCM-Ber2	GPTCM-MRF1	GPTCM-MRF2
Survival function	$S_{pop}(t) = e^{-\theta\{1-\sum_{l=1}^L \mathbf{p}_l S_l(t)\}}$ $S_l(t) = e^{-(t/\lambda_l)^\kappa}, \ l = 1, \dots, L$ $\lambda_l = \frac{\boldsymbol{\mu}_l}{\Gamma(1 + 1/\kappa)}$ $\kappa \sim \mathcal{Gamma}(a_\kappa, b_\kappa)$					
Cure fraction	$\log \theta = \xi_0 + \mathbf{X}_0 \boldsymbol{\xi}, \text{ where } \boldsymbol{\xi} = \{\xi_k\}_k, \ k = 1, \dots, d$ $\xi_0 \sim \mathcal{N}(0, v_0^2), \ v_0^2 \sim \mathcal{IGamma}(a_{v_0}, b_{v_0})$ $\xi_k \sim \mathcal{N}(0, v^2), \ v^2 \sim \mathcal{IGamma}(a_v, b_v)$					
Noncure fraction	$\log \boldsymbol{\mu}_l = \beta_{0l} + \mathbf{X}_l \boldsymbol{\beta}_l, \text{ where } \boldsymbol{\beta}_l = \{\beta_{jl}\}_{jl}, \ j = 1, \dots, p$ $\beta_{0l} \sim \mathcal{N}(0, \tau_0^2)$					
	Normal prior: $\beta_{jl} \sim \mathcal{N}(0, \tau_l^2), \ j = 1, \dots, p, \ l = 1, \dots, L$ $\tau_l^2 \sim \mathcal{IGamma}(a_\tau, b_\tau)$	Spike-and-slab prior: $\beta_{jl} \gamma_{jl}, \tau_l^2 \sim \gamma_{jl}\mathcal{N}(0, \tau_l^2) + (1 - \gamma_{jl})\delta_0(\beta_{jl})$ Bernoulli-beta: $\gamma_{jl} \pi_{jl} \sim \mathcal{Bernoulli}(\pi_{jl})$ $\pi_{jl} \sim \mathcal{Beta}(a_\pi, b_\pi)$ $\tau_l^2 \sim \mathcal{IGamma}(a_\tau, b_\tau)$		Spike-and-slab prior: $\beta_{jl} \gamma_{jl}, \tau_l^2 \sim \gamma_{jl}\mathcal{N}(0, \tau_l^2) + (1 - \gamma_{jl})\delta_0(\beta_{jl})$ MRF prior: $f(\boldsymbol{\gamma} a, b, G) \propto \exp\{a \mathbf{1}^\top \boldsymbol{\gamma} + b \boldsymbol{\gamma}^\top G \boldsymbol{\gamma}\}$ $\boldsymbol{\gamma} = (\gamma_{11}, \gamma_{12}, \dots, \gamma_{pL})^\top$ $\tau_l^2 \sim \mathcal{IGamma}(a_\tau, b_\tau)$		
Measurement error	$\tilde{\mathbf{p}} = \mathbf{p} + \text{No error}$ Observed proportions: $\tilde{\mathbf{p}} = [\tilde{\mathbf{p}}_1, \dots, \tilde{\mathbf{p}}_L]$ Underlying proportions: $\mathbf{p} = [\mathbf{p}_1, \dots, \mathbf{p}_L]$	$\tilde{\mathbf{p}} = \mathbf{p} + \text{Dirichlet error}^\dagger$ $f(\tilde{\mathbf{p}} \boldsymbol{\alpha}) = \frac{1}{\mathbf{B}(\boldsymbol{\alpha})} \prod_{l=1}^L \tilde{\mathbf{p}}_l^{\alpha_l - 1}$ $\mathbf{p}_l = \frac{\alpha_l}{\sum_{l'=1}^L \alpha_{l'}}$ $\log \alpha_l = \zeta_{0l} + \mathbf{X}_l \boldsymbol{\zeta}_l$ $\zeta_{0l} w_0^2 \sim \mathcal{N}(0, w_0^2)$ $\boldsymbol{\zeta}_l = \{\zeta_{jl}\}_{jl}$ $\zeta_{jl} w_l^2 \sim \mathcal{N}(0, w_l^2)$ $w_l^2 \sim \mathcal{IGamma}(a_w, b_w)$	$\tilde{\mathbf{p}} = \mathbf{p} + \text{No error}$	$\tilde{\mathbf{p}} = \mathbf{p} + \text{Dirichlet error}$ $f(\tilde{\mathbf{p}} \boldsymbol{\alpha}) = \frac{1}{\mathbf{B}(\boldsymbol{\alpha})} \prod_{l=1}^L \tilde{\mathbf{p}}_l^{\alpha_l - 1}$ $\log \alpha_l = \zeta_{0l} + \mathbf{X}_l \boldsymbol{\zeta}_l$ $\zeta_{0l} w_0^2 \sim \mathcal{N}(0, w_0^2)$ Spike-and-slab prior: $\zeta_{jl} \eta_{jl}, w_l^2 \sim \eta_{jl}\mathcal{N}(0, w_l^2) + (1 - \eta_{jl})\delta_0(\zeta_{jl})$ Bernoulli-beta: $\eta_{jl} \rho_{jl} \sim \mathcal{Bernoulli}(\rho_{jl})$ $\rho_{jl} \sim \mathcal{Beta}(a_\rho, b_\rho)$ $w_l^2 \sim \mathcal{IGamma}(a_w, b_w)$	$\tilde{\mathbf{p}} = \mathbf{p} + \text{Dirichlet error}$ $f(\tilde{\mathbf{p}} \boldsymbol{\alpha}) = \frac{1}{\mathbf{B}(\boldsymbol{\alpha})} \prod_{l=1}^L \tilde{\mathbf{p}}_l^{\alpha_l - 1}$ $\log \alpha_l = \zeta_{0l} + \mathbf{X}_l \boldsymbol{\zeta}_l$ $\zeta_{0l} w_0^2 \sim \mathcal{N}(0, w_0^2)$ Spike-and-slab prior: $\zeta_{jl} \eta_{jl}, w_l^2 \sim \eta_{jl}\mathcal{N}(0, w_l^2) + (1 - \eta_{jl})\delta_0(\zeta_{jl})$ MRF prior: $f(\boldsymbol{\eta} a^*, b^*, G^*) \propto \exp\{a^* \mathbf{1}^\top \boldsymbol{\eta} + b^* \boldsymbol{\eta}^\top G^* \boldsymbol{\eta}\}$ $w_l^2 \sim \mathcal{IGamma}(a_w, b_w)$	

Note:  $^\dagger$ The notation “ $\tilde{\mathbf{p}} = \mathbf{p} + \text{Dirichlet error}$ ” means that the proportions data  $\tilde{\mathbf{p}}$  follow a Dirichlet distribution with mean parameters  $\mathbf{p}$ .

## 2.2 Bayesian GPTCMs

### GPTCM-noBVS1

A simple version of GPTCM with covariates (denoted as GPTCM-noBVS1 in Table 1) is to introduce  $d$  mandatory variables  $\mathbf{X}_0 \in \mathbb{R}^{n \times d}$  into the cure fraction through the log-linear submodel (2), and introduce cell-type-specific covariates into the Weibull's mean parameter  $\boldsymbol{\mu}_l$  through another log-linear submodel:

$$\log \boldsymbol{\mu}_l = \beta_{0l} + \mathbf{X}_l \boldsymbol{\beta}_l, \quad l = 1, \dots, L, \quad (3)$$

where  $\mathbf{X}_l \in \mathbb{R}^{n \times p}$  includes  $p$  cell-type-specific covariates, and coefficients  $\boldsymbol{\beta}_l = (\beta_{1l}, \dots, \beta_{pl})^\top$ . By convention, for the log-linear submodel (2), a normal prior is used for the intercept  $\xi_0 \sim \mathcal{N}(0, v_0^2)$ , and another normal prior for each variable's effect, i.e.  $\xi_k \sim \mathcal{N}(0, v^2)$ ,  $k = 1, \dots, d$ . Similarly, for the log-linear submodel (3), normal priors are used for  $\beta_{0l}$  and  $\beta_{jl}$ :

$$\beta_{0l} \sim \mathcal{N}(0, \tau_0^2), \quad \beta_{jl} \sim \mathcal{N}(0, \tau_l^2), \quad l = 1, \dots, L, \quad j = 1, \dots, p.$$

Here, the cell-type-specific prior variances  $\tau_l^2$  allow different scales of cell-type-specific effects. Independent inverse-gamma priors can be used for all variances in the normal priors. This Bayesian version of GPTCM can be suited to handle low-dimensional covariates without the need of Bayesian variable selection (BVS).

### GPTCM-noBVS2

The GPTCM (1) assumes that after an initial treatment the numbers of multiple tumor cell subtypes follow a multinomial distribution given known cell type proportions  $\mathbf{p} = [\mathbf{p}_1, \dots, \mathbf{p}_L]$ . However, the true cell type proportions may not be measured accurately in real applications. We can assume that the measured proportions of multiple cell types  $\tilde{\mathbf{p}} = [\tilde{\mathbf{p}}_1, \dots, \tilde{\mathbf{p}}_L]$  follow a Dirichlet distribution with expectations as the underlying probabilities  $\mathbf{p}$ . Then we can use a measurement error model for the measured proportions data  $\tilde{\mathbf{p}}$ :

$$f(\tilde{\mathbf{p}}|\boldsymbol{\alpha}) = \frac{1}{B(\boldsymbol{\alpha})} \prod_{l=1}^L \tilde{\mathbf{p}}_l^{\alpha_l - 1}, \quad \mathbf{p}_l = \mathbb{E}[\tilde{\mathbf{p}}_l] = \frac{\alpha_l}{\sum_{l'=1}^L \alpha_{l'}},$$

where the concentration parameters  $\boldsymbol{\alpha} = (\alpha_1, \dots, \alpha_L)$ ,  $\alpha_l > 0$ ,  $B(\boldsymbol{\alpha})$  is a multivariate beta function, i.e.  $B(\boldsymbol{\alpha}) = \prod_{l=1}^L \Gamma(\alpha_l) / \Gamma(\sum_{l=1}^L \alpha_l)$ ,  $\Gamma(\cdot)$  is the gamma function. Cell-type-specific covariates can be introduced into the Dirichlet distribution via its concentration parameters, similar to the Dirichlet regression with the common parametrization (Maier, 2014):

$$\log \alpha_l = \zeta_{0l} + \mathbf{X}_l \boldsymbol{\zeta}_l, \quad l = 1, \dots, L.$$

The ideal of using the measurement error submodel is similar to the joint models (Faucett and Thomas, 1996). Similar to GPTCM-noBVS1, this version of GPTCM (denoted as GPTCM-noBVS2 shown in Table 1) can be suited to handle low-dimensional covariates without BVS.

### GPTCM-Ber1

In order to analyze high-dimensional covariates, particularly for identifying cell-type specific genes relevant in cancer research, we can employ independent spike-and-slab priors for the coefficients  $\beta_{jl}$  linked to the

mean parameters of cell-type-specific Weibull distributions in (3):

$$\begin{aligned}\beta_{jl}|\gamma_{jl}, \tau_l^2 &\sim \gamma_{jl}\mathcal{N}(0, \tau_l^2) + (1 - \gamma_{jl})\delta_0(\beta_{jl}), \\ \gamma_{jl} &\sim \text{Bernoulli}(\pi_{jl}),\end{aligned}\tag{4}$$

where  $\gamma_{jl}$  ( $l = 1, \dots, L; j = 1, \dots, p$ ) is a latent variable (with a Bernoulli hyperprior) for variable selection indicating  $\beta_{jl} \neq 0$  if  $\gamma_{jl} = 1$  and  $\beta_{jl} = 0$  if  $\gamma_{jl} = 0$ ,  $\tau_l^2$  is a shrinkage parameter with hyperprior  $\tau_l^2 \sim \mathcal{IG}(a_\tau, b_\tau)$ , and  $\delta_0(\cdot)$  is the Dirac delta function. We specify a beta hyperprior on the Bernoulli's probability  $\pi_{jl} \sim \text{Beta}(a_\pi, b_\pi)$ .

### GPTCM-Ber2

Similar to GPTCM-Ber1, we can also implement BVS for covariates linked to the cell-type-specific proportions in the measurement error submodel:

$$\begin{aligned}\log \alpha_l &= \zeta_{0l} + \mathbf{X}_l \boldsymbol{\zeta}_l, \\ \zeta_{jl}|\eta_{jl}, w_l^2 &\sim \eta_{jl}\mathcal{N}(0, w_l^2) + (1 - \eta_{jl})\delta_0(\zeta_{jl}), \\ \eta_{jl}|\rho_{jl} &\sim \text{Bernoulli}(\rho_{jl}), \\ \rho_{jl} &\sim \text{Beta}(a_\rho, b_\rho),\end{aligned}$$

where  $\eta_{jl}$ 's are latent indicators of variable selection for covariates linked to the Dirichlet's concentration parameters, and the Bernoulli-beta prior is also used for  $\eta_{jl}$ ,  $l = 1, \dots, L$ ,  $j = 1, \dots, p$ . This model is denoted as GPTCM-Ber2 shown in Table 1.

### GPTCM-MRF1

Alternative to the data-driven spike-and-slab priors for variable selection in (4), we can make use of prior knowledge of intercellular networks/pathways by employing graph-structured priors for variable selection. A Markov random field prior (MRF) (Li and Zhang, 2010; Stingo et al., 2011; Zhao et al., 2024a) can be used for the latent indicators of the effects  $\beta_l$  in (3) for variable selection and simultaneously addressing known relationships between cell-type-specific covariates. The MRF prior is for the vector of all latent indicators, i.e.  $\boldsymbol{\gamma} = \text{vec}[(\gamma_1, \dots, \boldsymbol{\gamma}_l, \dots, \boldsymbol{\gamma}_L)] = (\gamma_{11}, \gamma_{21}, \dots, \gamma_{pL})^\top$ ,  $\boldsymbol{\gamma}_l = (\gamma_{1l}, \dots, \gamma_{pl})^\top$ ,  $l = 1, \dots, L$ :

$$f(\boldsymbol{\gamma}|a, b, G) \propto \exp\{a\mathbf{1}^\top \boldsymbol{\gamma} + b\boldsymbol{\gamma}^\top G \boldsymbol{\gamma}\},\tag{5}$$

where  $a < 0$  controls overall model sparsity,  $b \geq 0$  determines the strength of the structure relationships between variables, and  $G$  is an  $pL \times pL$  adjacency or weight matrix representing a graph corresponding to the known structure relationships between variables. If  $b = 0$ , the MRF prior is degenerated to independent Bernoulli priors for individual variable selection indicators. The full model is denoted as GPTCM-MRF1 shown in Table 1.

### GPTCM-MRF2

Similar to GPTCM-MRF1 with graph-structured priors for the BVS of covariates linked to cell-type-specific survival only, we can also employ the graph-structured priors for the BVS of covariates linked to cell-type-specific proportions in the measurement error submodel:

$$f(\boldsymbol{\eta}|a^*, b^*, G^*) \propto \exp\{a^*\mathbf{1}^\top \boldsymbol{\eta} + b^*\boldsymbol{\eta}^\top G^* \boldsymbol{\eta}\},$$

where the vector of all indicator variables  $\boldsymbol{\eta} = \text{vec}[(\boldsymbol{\eta}_1, \dots, \boldsymbol{\eta}_l, \dots, \boldsymbol{\eta}_L)] = (\eta_{11}, \eta_{21}, \dots, \eta_{pL})^\top$ ,  $\boldsymbol{\eta}_l = (\eta_{1l}, \dots, \eta_{pl})^\top$ , parameters  $a^*$  and  $b^*$  control the model sparsity and strength of prior graph knowledge  $G^*$ , respectively. Note that the graph  $G^*$  here can be the same as the graph  $G$  in (5), if we do not have another prior biological knowledge to distinguish the relationships between the cell-type-specific survival related effects and the cell-type-specific proportions related effects. The full model is denoted as GPTCM-MRF2 shown in Table 1.

## 2.3 Computation

We consider a survival modeling framework for right-censored time-to-event data. Let  $T_i$  and  $C_i$ ,  $i = 1, \dots, n$ , be the times to tumor progression and censoring for the  $i$ -th subject, respectively. The observed time  $T_i^* = \min\{T_i, C_i\}$  and the censoring indicator  $\delta_i = \mathbb{1}\{T_i \leq C_i\}$ . We consider commonly used assumptions: (i) independence between  $T_i$  and  $C_i$ , (ii) independence between  $(T_i, C_i)$  and  $(T_j, C_j)$  for  $1 \leq i \neq j \leq n$ , (iii) non-informative censoring, and cure rate  $\mathbb{P}(N = 0) = e^{-\theta}$ ,  $\theta > 0$ . Let  $f(t_i|\mathcal{D})$  be a ‘‘conceptual’’ likelihood at a time point for the  $i$ -th individual, and then the likelihood function for the entire population is

$$\mathcal{L}(\boldsymbol{\theta}|\mathcal{D}) = \prod_{i=1}^n f(t_i|\mathcal{D})f(\tilde{\mathbf{p}}_i|\mathbf{p}_i) \propto \prod_{i=1}^n f_{pop}(t_i|\boldsymbol{\mathcal{X}}_i, \mathbf{p}_i)^{\delta_i} S_{pop}(t_i|\boldsymbol{\mathcal{X}}_i, \mathbf{p}_i)^{1-\delta_i} f(\tilde{\mathbf{p}}_i|\mathbf{p}_i), \quad (6)$$

where  $\boldsymbol{\theta}$  consists of all relevant parameters,  $\mathcal{D} = \{t_i, \delta_i, \boldsymbol{\mathcal{X}}_i, \tilde{\mathbf{p}}_i\}_{i=1}^n$  is the observed data,  $f_{pop}(t_i|\boldsymbol{\mathcal{X}}_i) = -\frac{d}{dt}S_{pop}(t_i|\boldsymbol{\mathcal{X}}_i)$  is the probability density function corresponding to the population survival function, and  $\boldsymbol{\mathcal{X}}_i = \{\mathbf{X}_{i0}, \mathbf{X}_{i1}, \dots, \mathbf{X}_{il}, \dots, \mathbf{X}_{iL}\}$  consists of clinical covariates and cell-type-specific covariates. Note that  $S_{pop}(t)$  is not a proper survival function, so  $f_{pop}(t_i|\boldsymbol{\mathcal{X}}_i)$  is not a proper probability density function.

To proceed with posterior computation for GPTCM-MRF2 as an example, we assume mutual independence among the prior of the Weibull’s shape parameter and the priors of the coefficients in cure and noncure fractions. The joint posterior distribution is composed by the likelihood (6) and the joint distribution of hyperparameters, i.e.

$$\begin{aligned} f(\boldsymbol{\theta}|\mathcal{D}) &\propto \mathcal{L}(\boldsymbol{\theta}|\mathcal{D})f(\boldsymbol{\theta}) \\ &= \mathcal{L}(\boldsymbol{\theta}|\mathcal{D})f(\boldsymbol{\xi}, \xi_0, v^2, v_0^2, \kappa, \boldsymbol{\beta}, \beta_0, \boldsymbol{\tau}^2, \tau_0^2, \boldsymbol{\gamma}, G, \boldsymbol{\zeta}, \zeta_0, \boldsymbol{w}^2, w_0^2, \boldsymbol{\eta}, G^*) \\ &= \mathcal{L}(\boldsymbol{\theta}|\mathcal{D}) \prod_{k=1}^d \{f(\xi_k|v^2)\} f(v^2) f(\xi_0|v_0^2) f(v_0^2) f(\kappa) \prod_{l=1}^L \{f(\beta_l|\gamma_l, \boldsymbol{\tau}_l) f(\boldsymbol{\tau}_l) f(\beta_{0l}|\tau_0^2) f(\tau_0^2)\} f(\boldsymbol{\gamma}|G) \\ &\quad \times \prod_{l=1}^L \{f(\zeta_l|\boldsymbol{\eta}_l, \boldsymbol{w}) f(\boldsymbol{w}) f(\zeta_{0l}|w_0^2) f(w_0^2)\} f(\boldsymbol{\eta}|G^*) \\ &= \prod_{i=1}^n f_{pop}(t_i|X_i, \mathbf{p}_i)^{\delta_i} S_{pop}(t_i|X_i, \mathbf{p}_i)^{1-\delta_i} f(\tilde{\mathbf{p}}_i|\mathbf{p}_i) \prod_{k=1}^d \{f(\xi_k|v^2)\} f(v^2) f(\xi_0|v_0^2) f(v_0^2) f(\kappa) \\ &\quad \times \prod_{l=1}^L \left\{ \prod_{j=1}^p \{f(\beta_{jl}|\gamma_{jl}, \tau_l^2) f(\tau_l^2) f(\beta_{0l}|\tau_0^2) f(\tau_0^2)\} \right\} f(\boldsymbol{\gamma}|G) \\ &\quad \times \prod_{l=1}^L \left\{ \prod_{j=1}^p \{f(\zeta_{jl}|\eta_{jl}, w_l^2) f(w_l^2) f(\zeta_{0l}|w_0^2) f(w_0^2)\} \right\} f(\boldsymbol{\eta}|G^*). \end{aligned}$$

All relevant full conditionals can be found in Supplementary material S1. For simple full conditionals

with beta and inverse-gamma distributions, we use Gibbs sampling. Since the full conditionals of  $\beta = \text{vec}[(\beta_1, \dots, \beta_L)]$  and  $\zeta = \text{vec}[(\zeta_1, \dots, \zeta_L)]$  are log-concave and can be for high-dimensional parameters, we update them by using the adaptive rejection Metropolis sampling (ARMS) (Gilks et al., 1995). For the latent indicators  $\gamma$  and  $\eta$  for variable selection, we use Thompson sampling (Thompson, 1933). For computational efficiency, every time we update the latent indicators for variable selection corresponding to one randomly chosen cell type only. For other full conditionals with complex densities, we use slice sampling (Neal, 2003). Algorithm 1 shows the Markov chain Monte Carlo (MCMC) for fitting GPTCM-MRF2. The algorithm is also used for other Bayesian versions of GPTCM with slight changes based on different priors.

---

**Algorithm 1** : MCMC for GPTCM-MRF2

---

- 1: Set hyperparameters  $a_v, b_v, a_{v_0}, b_{v_0}, a_\tau, b_\tau, a_{\tau_0}, b_{\tau_0}, a_w, b_w, a_{w_0}, b_{w_0}, a_\kappa, b_\kappa, G, G^*, a, b, a^*, b^*$
  - 2: Initialize coefficients  $\xi_0, \xi, \beta_l$  and  $\gamma_l$  ( $l = 1, \dots, L$ )
  - 3: Set the number of iterations  $M$
  - 4: **for**  $i = 1, \dots, M$  **do**
  - 5:     Draw  $v_0^2$  and  $v^2$  via Gibbs sampling
  - 6:     Draw  $\xi_0$  and  $\xi_k$  ( $k = 1, \dots, d$ ) via slice sampling
  - 7:     Update cure fraction rate  $\theta = \exp\{\xi_0 + \mathbf{X}_0 \xi\}$
  - 8:     Randomly draw one  $l$  from  $\{1, \dots, L\}$
  - 9:         Draw  $\eta_l$  via Thompson sampling
  - 10:         Draw  $w_l^2$  and  $w_0^2$  via Gibbs sampling
  - 11:         Draw  $\zeta_l$  corresponding to nonzero elements of  $\eta_l$  and  $\zeta_{0l}$  via ARMS
  - 12:     Draw all  $\zeta_l$  via ARMS,  $\forall l$
  - 13:     Update Dirichlet mean proportions  $\mathbf{p}_l = \frac{\alpha_l}{\sum_{l'=1}^L \alpha_{l'}}$ , where  $\alpha_l = \exp\{\zeta_{0l} + \mathbf{X}_l \zeta_l\}$ ,  $\forall l$
  - 14:     Draw Weibull's shape parameter  $\kappa$  via slice sampling, and update  $\lambda_l = \frac{\mu_l}{\Gamma(1+1/\kappa)}$ ,  $S_l(t) = \exp\{-(t/\lambda_l)^\kappa\}$ ,  $\forall l$
  - 15:     Randomly draw one  $l$  from  $\{1, \dots, L\}$
  - 16:         Draw  $\gamma_l$  via Thompson sampling
  - 17:         Draw  $\tau_l^2$  and  $\tau_0^2$  via Gibbs sampling
  - 18:         Draw  $\beta_l$  corresponding to nonzero elements of  $\gamma_l$  and  $\beta_{0l}$  via ARMS
  - 19:     Draw all  $\beta_l$  via ARMS,  $\forall l$
  - 20:     Update Weibull's mean parameter  $\mu_l = \exp\{\beta_{0l} + \mathbf{X}_l \beta_l\}$ , and update  $\lambda_l$  and  $S_l(t)$
  - 21: **end for**
- 

### Specification of hyperparameters

For the Weibull's shape parameter, we use a non-informative prior  $\kappa \sim \mathcal{Gamma}(1, 1)$ . As a practical suggestion, all the covariates can be standardized, i.e. transforming to  $z$ -score values. Since a weakly informative inverse-gamma prior is used for each variance (i.e.  $v_0^2, v^2, \tau_0^2, \tau_l^2, w_0^2, w_l^2$ ), we set a prior  $\mathcal{IGamma}(5, 20)$  by default. If the magnitude of some covariates is very large, the inverse-gamma prior can be specified with a large variance. For GPTCM-Ber1 and GPTCM-Ber2 with the Bernoulli-beta prior, the Bernoulli's probability is assigned by a beta prior  $\mathcal{Beta}(1, cp)$ , where  $p$  is the number of cell-type-specific covariates, and  $c > 0$  is a tuning parameter. For GPTCM-MRF1 and GPTCM-MRF2 with a MRF prior, the sparsity parameter (i.e.  $a$  or  $a^*$ ) is chosen according to the logistic transformation with an assumed model sparsity  $s$ , i.e.  $a = \text{logit}(s)$ , since the MRF prior is reduced to independent Bernoulli priors with probability  $\text{logit}^{-1}(s)$  if  $b = 0$ . The MRF hyperparameter  $b$  or  $b^*$  for the strength of the structure relationships between variables is tuned via a grid search. The graph matrix ( $G$  or  $G^*$ ) in the MRF prior is a weight matrix with weight 1 between two linked variables in a given biological network/pathway and weight 0.5 (or any value between



0 and 1) between two variables that are naturally correlated (e.g. the same gene with different representations in different cell types). For the tuning parameters, their optimal values can be chosen based on the criteria of the expected log pointwise predictive density (elpd) calculated by the approximate leave-one-out cross-validation (Vehtari et al., 2024).

### 3 Simulations

We use simulations to gain insight into the performance of the proposed Bayesian GPTCMs, as well as comparisons with classical survival methods. We simulate  $L = 3$  cell types with both low-dimensional ( $p = 10, n = 200$ ) and high-dimensional cell-type-specific covariates ( $p = 200, n = 200$ )  $\mathbf{X}_l \in \mathbb{R}^{n \times p}$ ,  $l = 1, \dots, L$ , and assume only a few covariates are truly relevant. The cure rate parameter is modeled by two mandatory covariates  $\mathbf{X}_0 = \{x_{(0)i1}, x_{(0)i2}\}_{i=1}^n$  via a logarithmic link function. Censoring is generated through an exponential distribution that results in approximately 20% censoring rate. See below the simulation scheme:

$$\begin{aligned}
x_{(0)i1} &\sim \text{Bern}(0.5), \quad x_{(0)i2} \sim \mathcal{N}(0, 1), \quad i = 1, \dots, n \\
\theta_i &= \exp\{1 + 0.6x_{(0)i1} - x_{(0)i2}\} \\
\text{vec}[(\mathbf{X}_{i1}, \dots, \mathbf{X}_{iL})] &\sim \mathcal{N}(0, \Sigma), \quad \mathbf{X}_{il} = (x_{i1l}, \dots, x_{ipl})^\top, \quad l = 1, \dots, L \\
\mu_{il} &= \exp\{\mathbf{X}_{il}\boldsymbol{\beta}_l\} \\
\alpha_{il} &= \exp\{\zeta_{0l} + \mathbf{X}_{il}\boldsymbol{\zeta}_l\} \\
\mathbf{p}_{i\cdot} &= (\mathbf{p}_{i1}, \dots, \mathbf{p}_{iL}) \sim \text{Dirichlet}(\alpha_{i1}, \dots, \alpha_{iL}) \\
C_i^1 &\sim \text{Uniform}(1, 4) \\
C_i^2 &\sim \text{Exponential}(-\log(0.8)/5) \\
C_i &= \min\{C_i^1, C_i^2\} \\
U_i &\sim \text{Uniform}(0, 1) \\
T_i &= \begin{cases} +\infty, & U_i \leq e^{-\theta_i} \\ \text{Metropolis-Hastings sampler for } S_{pop}(t), & U_i > e^{-\theta_i} \end{cases} \\
T_i^* &= \min\{T_i, C_i\} \\
\delta_i &= \mathbb{1}\{T_i \leq C_i\}.
\end{aligned}$$

Note that to simulate  $U_i$  above is for generating the cured population. If  $U_i \leq e^{-\theta_i}$ , then the  $i$ -th subject was censored, so the observed time  $T_i^*$  is equal to the censored time  $C_i$  smaller than the true survival time, i.e.  $T_i^* = \min\{T_i, C_i\} = C_i$ , and no event happened  $\delta_i = 0$ . The Weibull's shape parameter is set as  $\kappa = 2$ . The covariance matrix of the cell-type-specific covariates is set as

$$\Sigma = \begin{pmatrix} \Sigma_1 & \varrho \mathbb{I}_p & \cdots & \varrho \mathbb{I}_p \\ \varrho \mathbb{I}_p & \Sigma_2 & \cdots & \varrho \mathbb{I}_p \\ \vdots & \vdots & \ddots & \vdots \\ \varrho \mathbb{I}_p & \varrho \mathbb{I}_p & \cdots & \Sigma_L \end{pmatrix}.$$

The diagonals of the covariance matrix  $\Sigma$  are 1. In the off-diagonal blocks of  $\Sigma$ ,  $\varrho = 0.1$  meaning that the correlation between the same gene with different gene expression levels from any two cell types is 0.1. In the

$l$ -th block diagonal matrix,  $\Sigma_l = \{\sigma_{jj'l}\}_{jj'}$  with  $\sigma_{jj'l} = \varrho_l^{|j-j'|}$  if  $j, j' \leq 6$  and  $\sigma_{jj'l} = 0$  otherwise,  $\varrho_1 = 0.13$ ,  $\varrho_2 = 0.14$  and  $\varrho_3 = 0.15$ . The effects of cell-type-specific covariates are set as

$$\begin{aligned}\beta_1 &= (-1.0, -0.5, 0.8, 0.8, -1.0, 0, 0, \underbrace{0, \dots, 0}_{\#p-7})^\top, \\ \beta_2 &= (0, -0.9, -0.8, 0, 1.5, 1, 0, \underbrace{0, \dots, 0}_{\#p-7})^\top, \\ \beta_3 &= (1.0, 0, -0.4, -1.5, 0, 0, 0.8, \underbrace{0, \dots, 0}_{\#p-7})^\top, \\ \zeta_1 &= (0.7, -0.7, 0.5, -0.5, 1, 0, 0, \underbrace{0, \dots, 0}_{\#p-7})^\top, \\ \zeta_2 &= (-0.5, 0.5, 0, 1, 0, -1, 0, \underbrace{0, \dots, 0}_{\#p-7})^\top, \\ \zeta_3 &= (0, 0, 1, -0.5, -0.7, 0, 0, \underbrace{0, \dots, 0}_{\#p-7})^\top.\end{aligned}$$

The intercepts in the measurement error submodel for the Dirichlet concentration parameters are set as  $(\zeta_{01}, \zeta_{02}, \zeta_{03}) = (-.5, 1, 1.2)$ . We simulate additionally independent  $n = 200$  samples as validation data to assess the prediction performance of all models.

Furthermore, we simulate data from a Cox proportional hazards model to assess the performance of the proposed Bayesian GPTCMs under model misspecification. Five covariates are simulated independently from a standard normal distribution, with the number of subjects  $n = 200$ . The effects of the five covariates are set as  $(-0.8, -2, -2, 1, 1)$ . The survival data are simulated based on the Cox-Weibull model (Bender et al., 2005) with the Weibull's shape parameter  $\kappa = 2$  and the censoring rate is controlled as approximately 20%.

### 3.1 Simulation results in low dimensions

We compare the six Bayesian versions of the GPTCM proposed in Section 2 as well as the classical Cox model (Cox, 1972) and the semiparametric promotion time cure model (PTCM) (Ma and Yin, 2008). Note that the Cox model and PTCM are not suited to model the cell-type proportions data. We implemented three versions of the Cox model: (i) "Cox-X0": with only clinical covariates  $\mathbf{X}_0$ , (ii) "Cox-Xmean": with mean aggregate covariates of  $\mathbf{X}_1, \dots, \mathbf{X}_L$ , i.e. each covariate is the mean of the corresponding  $L$  cell-type-specific covariates, and (iii) "Cox-X0-Xmean": with both covariates from (i) and (ii). For the semiparametric PTCM, only the clinical variables were included for modeling the cure fraction, denoted as "PTCM-X0". For the GPTCMs with a MRF prior (i.e. GTPCM-MRF1 and GTPCM-MRF2), a graph based on the precision matrix  $\Sigma^{-1}$  was used, which has weights 1 corresponding to nonzero entries of the precision matrix but weights 0.5 corresponding to the same variable with  $L$  representative features in different cell types. For each of the six GPTCMs, we ran 25,000 MCMC iterations with the first 5,000 iterations as a warmup period.

Figure 1 shows the survival prediction in terms of time-dependent Brier score by all models based on a validation data set. Figure 1 indicates the superior prediction performances of three GPTCMs (i.e. GPTCM-noBVS2, GPTCM-Ber2 and GPTCM-MRF2) that model covariates for both cell-type-specific survival and cell-type-specific proportions, in which GPTCM-Ber2 and GPTCM-MRF2 have exactly the same prediction performance, and GPTCM-noBVS2 has slightly worse prediction performance. The performances of three GPTCMs without modeling covariates for cell-type-specific proportions (i.e. GPTCM-noBVS1, GPTCM-

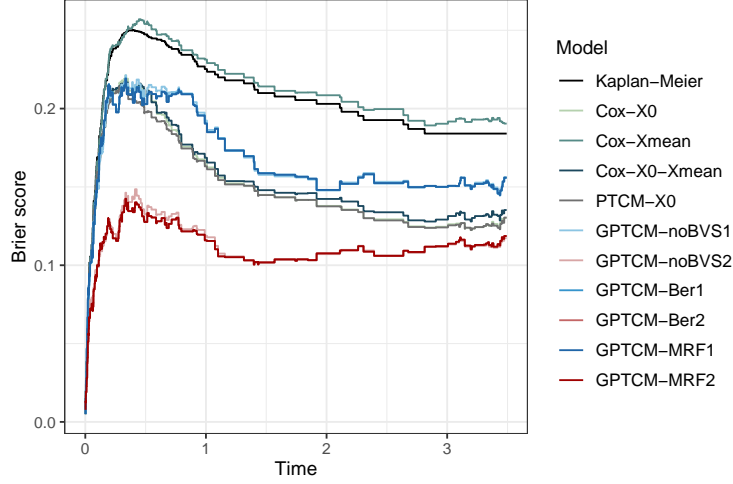


Figure 1: *Simulation results in low dimensions: Out-sample prediction errors of classical survival models and GPTCMs in terms of time-dependent Brier score. The Kaplan-Meier method is as a reference that did not account for any covariate. The method “Cox-X0” only models clinical covariates  $\mathbf{X}_0$ . The method “Cox-Xmean” models mean aggregate covariates of  $\mathbf{X}_1, \dots, \mathbf{X}_L$ . The method “Cox-X0-Xmean” models both clinical covariates  $\mathbf{X}_0$  and mean aggregate covariates of  $\mathbf{X}_1, \dots, \mathbf{X}_L$ . The predictions of GPTCM-noBVS1 and GPTCM-noBVS2 were based on the posterior mean of all parameters. The predictions of other GPTCMs were based on the estimates of their median probability models (MPMs) for the effects of covariates with variable selection and estimates of posterior mean for other parameters.*

Ber1 and GPTCM-MRF1) perform similarly to the classical models Cox-X0, Cox-X0-Xmean and PTCM-X0 for short-term survival predictions, but they become worse than those classical models for long-term survival predictions. The Cox model with only mean aggregate covariates omitting clinical covariates (i.e. Cox-Xmean) has worse prediction performance than the Kaplan-Meier method.

Figure 2 shows the posterior distributions of the effects on cell-type-specific survival and effects on cell-type-specific proportions by GPTCM-noBVS2 (Figure 2A-B) and GPTCM-MRF2 (Figure 2C-D). Although all the posterior distributions of the effects from GPTCM-noBVS2 (Figure 2A-B) cover the true effects almost, they have much larger variations than the posterior distributions from GPTCM-MRF2 (Figure 2C-D). In particular, GPTCM-MRF2 results in the estimates of the truly unrelated variables (true effects as zero) with very high densities at the value zero and the estimates of the truly related variables with most densities far away from the value zero, i.e. with accurate variable selection. Supplementary Figure S1A-B also shows that GPTCM-MRF2 results in the marginal posterior inclusion probabilities (mPIPs) of the truly unrelated variables close to 0 and the mPIPs of the truly related variables close to 1. GPTCM-Ber2 has similar performance to GPTCM-MRF2 in terms of variable selection and effect estimation, see Supplementary Figure S1C-D and Supplementary Figure S2. For other three GPTCMs with only modeling covariates for cell-type-specific survival (i.e. GPTCM-noBVS1, GPTCM-Ber1 and GPTCM-MRF1), GPTCM-noBVS1 performs similarly to GPTCM-noBVS2 in terms of the effects on cell-type-specific survival (Supplementary Figure S3A), and GPTCM-Ber1 and GPTCM-MRF1 perform similarly to GPTCM-Ber2 and GPTCM-MRF2 in terms of the posterior distributions of the effects on cell-type-specific survival (Supplementary Figure S3B-C).

Table 2 shows that the four GPTCMs with BVS (i.e. GPTCM-Ber1, GPTCM-Ber2, GPTCM-MRF1 and GPTCM-MRF2) slightly outperform GPTCM-noBVS1 and GPTCM-noBVS2 in terms of estimated

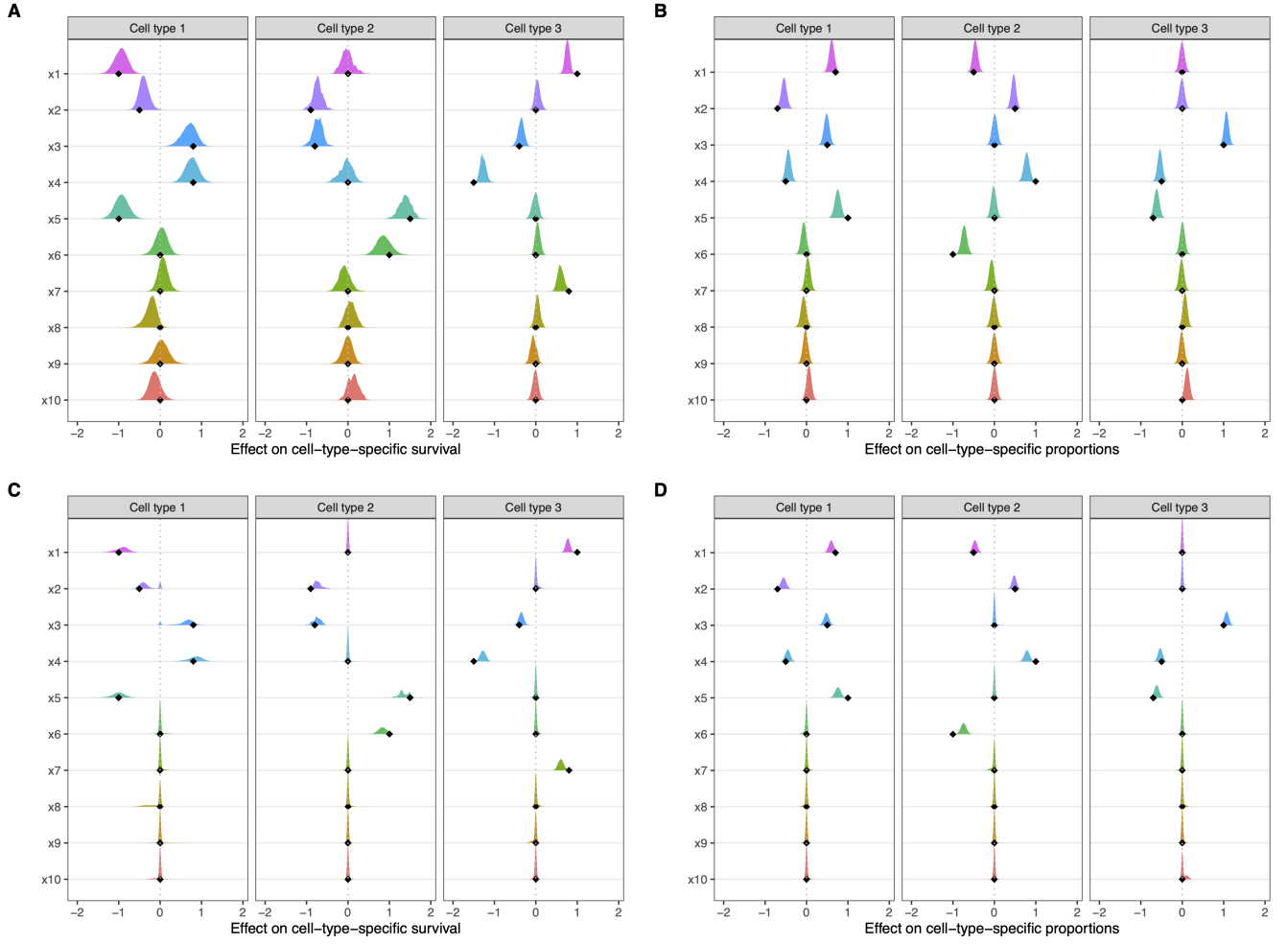


Figure 2: *Simulation results in low dimensions: Posterior distributions of the effects on cell-type-specific survival and proportions. The black colored diamond indicates the true effect. (A) Posterior distributions of the effects on cell-type-specific survival by GPTCM-noBVS2. (B) Posterior distributions of the effects on cell-type-specific proportions by GPTCM-noBVS2. (C) Posterior distributions of the effects on cell-type-specific survival by GPTCM-MRF2. (D) Posterior distributions of the effects on cell-type-specific proportions by GPTCM-MRF2.*

Table 2: Simulation results in low dimensions: Model estimation and variable selection

Model	$\frac{1}{\sqrt{pL}} \ \hat{\beta} - \beta\ _2$	$\frac{1}{\sqrt{pL}} \ \hat{\zeta} - \zeta\ _2$	Accuracy		Sensitivity		Specificity	
			$\gamma$	$\eta$	$\gamma$	$\eta$	$\gamma$	$\eta$
GPTCM-noBVS1	0.108							
GPTCM-noBVS2	0.109	0.095						
GPTCM-Ber1	0.097		1.000		1.000		1.000	
GPTCM-Ber2	0.092	0.086	1.000	1.000	1.000	1.000	1.000	1.000
GPTCM-MRF1	0.094		1.000		1.000		1.000	
GPTCM-MRF2	0.092	0.085	1.000	1.000	1.000	1.000	1.000	1.000

NOTE: The empty cells are due to no parameters in corresponding models. The variable selection performance (i.e. accuracy, sensitivity and specificity) of the last four GPTCMs (i.e. GPTCM-Ber1, GPTCM-Ber2, GPTCM-MRF1 and GPTCM-MRF2) is determined by the median probability model with mPIP thresholded at 0.5. Note that the uncertainty for the estimation of the variable selection related parameters can be seen in Figure 2, Supplementary Figure S1, Supplementary Figure S2 and Supplementary Figure S3.

effects on the cell-type-specific survival, i.e.  $\frac{1}{\sqrt{pL}} \|\hat{\beta} - \beta\|_2$ . In terms of the estimated effects on the cell-type-specific proportions,  $\frac{1}{\sqrt{pL}} \|\hat{\zeta} - \zeta\|_2$ , the two GPTCMs with BVS (i.e. GPTCM-Ber2 and GPTCM-MRF2) also slightly outperforms GPTCM-noBVS2. All the four GPTCMs with BVS (i.e. GPTCM-Ber1, GPTCM-Ber2, GPTCM-MRF1 and GPTCM-MRF2) based on their MPMs with mPIPs thresholded at 0.5 have well identified truly related and truly unrelated variables, see the variable selection accuracy, sensitivity and specificity in Table 2.

For the effect estimation of clinical variables, Figure 3 shows that all the six GPTCMs resulted in their 95% credible intervals of the two clinical variables' effects covering the true effect values. However, the three classical survival models (i.e. Cox-X0, Cox-X0-Xmean and PTCM-X0) estimated the second clinical variable's effect  $\xi_2$  badly.

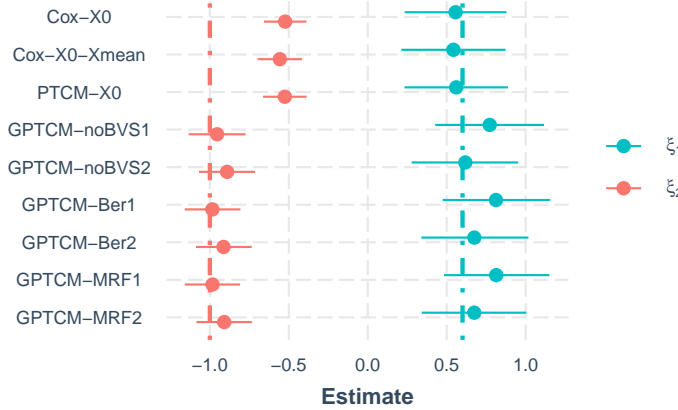


Figure 3: Simulation results in low dimensions: Estimates of the clinical variables' effects on the cure fraction. The solid circle point shows a point estimate (frequentist point estimate by Cox-X0, Cox-X0-Xmean or PTCM-X0, or posterior mean by GPTCMs). The error bar shows a 95% confidence interval (by Cox-X0, Cox-X0-Xmean or PTCM-X0) or a 95% credible interval (by GPTCMs). The green and red colored dot-dashed lines denote the true effects of the two clinical variables, respectively.

In addition, we simulated data based on a Cox proportional hazards model to assess the performance of GPTCMs under model misspecification. Since the underlying true model only includes five clinical variables, we fitted GPTCMs by including the five variables in both cure and noncure fractions. Since GPTCM-Ber2

and GPTCM-MRF2 also need proportions data as input data, we used pseudo proportions data of three cell types with all values 1/3. The MRF prior uses a graph matrix with nonzero weights 1 only for the same variable across the three pseudo cell types. Supplementary Figure S4 shows that the two classical survival models (i.e. Cox-X0, PTCM-X0) have the best prediction performances in terms of time-dependent Brier score. The four GPTCMs with BVS (i.e. GPTCM-Ber1, GPTCM-Ber2, GPTCM-MRF1 and GPTCM-MRF2) perform slightly worse than the classical survival models for short-term survival prediction, but their performances become much worse for long-term survival prediction. The other two GPTCMs without variable selection (i.e. GPTCM-noBVS1 and GPTCM-noBVS2) have much worse survival prediction than the Kaplan-Meier method (Supplementary Figure S4). From Supplementary Figure S5A-C, we see that the cell-type-specific effect estimates by GPTCM-noBVS1 and GPTCM-noBVS2 have very large variation. In contrast, the other four GPTCMs with BVS (i.e. GPTCM-Ber1, GPTCM-Ber2, GPTCM-MRF1 and GPTCM-MRF2) estimated all cell-type-specific effects with accurate value 0 as expected (Supplementary Figure S5D-I). For the effect estimation of the clinical covariates in the cure fraction, GPTCM-noBVS1 and GPTCM-noBVS2 result in largely variational estimated posterior distributions, with all 95% credible intervals covering the value 0. However, GPTCM-MRF1 and GPTCM-MRF2 result in estimates with narrow 95% credible intervals that cover the values of true effects and far away from 0 similar to the Cox model under the correct model specification (Supplementary Figure S6).

### 3.2 Simulation results in high dimensions

Since GPTCM-noBVS1, GPTCM-noBVS2 and classical survival models cannot deal with high-dimensional covariates, we compare the other four GPTCMs (i.e. GPTCM-Ber1, GPTCM-Ber2, GPTCM-MRF1 and GPTCM-MRF2), the classical Cox model with only clinical covariates, and two elastic net Cox models (Simon et al., 2011). Both the two elastic net Cox models include the clinical covariates as mandatory variables and perform variable selection for other high-dimensional covariates with an  $\ell_1/\ell_2$ -norm (or elastic net) penalty. The first elastic net Cox model (denoted as “elastic net1”) performs variable selection for the  $p$  mean aggregate covariates of  $\mathbf{X}_1, \dots, \mathbf{X}_L$ , but the second elastic net Cox model (denoted as “elastic net2”) performs variable selection for all  $pL$  individual cell-type-specific covariates  $[\mathbf{X}_1, \dots, \mathbf{X}_L]$ . The elastic net penalty parameters were optimized by using cross-validation. For the GPTCMs with a MRF prior (i.e. GPTCM-MRF1 and GPTCM-MRF2), a graph based on the precision matrix  $\Sigma^{-1}$  was used in the same way as the setting in low dimensions in Section 3.1. For each of the four GPTCMs, we ran 500,000 MCMC iterations with the first 200,000 iterations as a warmup period.

Figure 4 shows the survival prediction in terms of time-dependent Brier score by all models in high dimensions based on a validation data set. Figure 4 indicates the superior prediction performances of two GPTCMs (i.e. GPTCM-Ber2 and GPTCM-MRF2) that model covariates for both cell-type-specific survival and cell-type-specific proportions, in which GPTCM-MRF2 has slightly better prediction performance with lower Brier scores over time. The performances of the other two GPTCMs (i.e. GPTCM-Ber1 and GPTCM-MRF1) without modeling covariates for cell-type-specific proportions outperform the two elastic net models for short-term survival predictions (until time point 1.2), but they lead to worse long-term survival predictions (Figure 4). The elastic net1 estimated the effects of all mean aggregate covariates as zero, so that it results in the same model as the classical Cox model with only clinical covariates (i.e. Cox-X0) and has exactly the same prediction performance as Cox-X0 in Figure 4. However, elastic net2 with modeling all individual cell-type-specific covariates has slightly better survival prediction than elastic net1. Although the elastic net2 can induce variable selection from all individual cell-type-specific covariates, it only identified 15.4% of

truly related covariates (Table 3 with elastic net2’s sensitivity 0.154 corresponding to  $\gamma$ ).

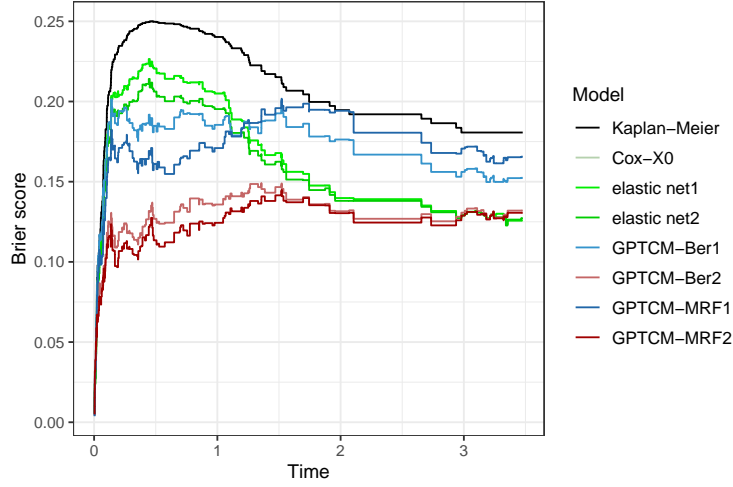


Figure 4: *Simulation results in high dimensions: Out-sample prediction errors of classical survival models and GPTCMs in terms of time-dependent Brier score. The Kaplan-Meier method is as a reference that did not account for any covariate. The elastic net Cox model “elastic net1” included the clinical variables  $\mathbf{X}_0$  and mean aggregate variables of  $\mathbf{X}_1, \dots, \mathbf{X}_L$ . The elastic net Cox model “elastic net2” included the clinical variables  $\mathbf{X}_0$  and all cell-type-specific variables  $[\mathbf{X}_1, \dots, \mathbf{X}_L]$ . The predictions of other GPTCMs were based on the estimates of their median probability models (MPMs) for the effects of covariates with variable selection and estimates of posterior mean for other parameters.*

Figure 5 shows that GPTCM-MRF2 results in reasonable mPIPs for covariate effects both on cell-type-specific survival and cell-type-specific proportions. Table 3 shows that GPTCM-MRF2 correctly identified all truly related covariates (i.e. with sensitivity 1.000 corresponding to  $\gamma$  and  $\eta$ ), and correctly identified most unrelated covariates with specificity 0.997 corresponding to  $\gamma$  (i.e. effects on cell-type-specific survival) and with specificity 1.000 corresponding to  $\eta$  (i.e. effects on cell-type-specific proportions). GPTCM-Ber2 has perfect variable selection and good estimation for covariate effects on cell-type-specific proportions, see Supplementary Figure S7 and Table 3 with GPTCM-Ber2’s sensitivity and specificity corresponding to  $\gamma$ , and  $\frac{1}{\sqrt{pL}} \|\hat{\zeta} - \zeta\|_2 = 0.022$ . But GPTCM-Ber2 without prior knowledge does not identify many truly related covariates linked to cell-type-specific survival, with sensitivity only 0.615 (Table 3). Supplementary Figure S9A-B show that GPTCM-Ber1 and GPTCM-Ber2 cannot capture a few nonzero effects on cell-type-specific survival corresponding to cell type 1 and cell type2, but GPTCM-MRF1 and GPTCM-MRF2 have better estimation (Supplementary Figure S9D-E).

For the effect estimation of clinical variables, Figure 6 shows that all the four GPTCMs resulted in their 95% credible intervals of the two clinical variables’ effects covering the true effect values and far away from value 0. The elastic net1 and elastic net2 models result in their the Bootstrapping 95% confidence intervals also covering the true effect values but with larger variation than the GPTCMs. However, the classical Cox model, Cox-X0, results in biased effect estimation of  $\xi_2$  for the second clinical variable.

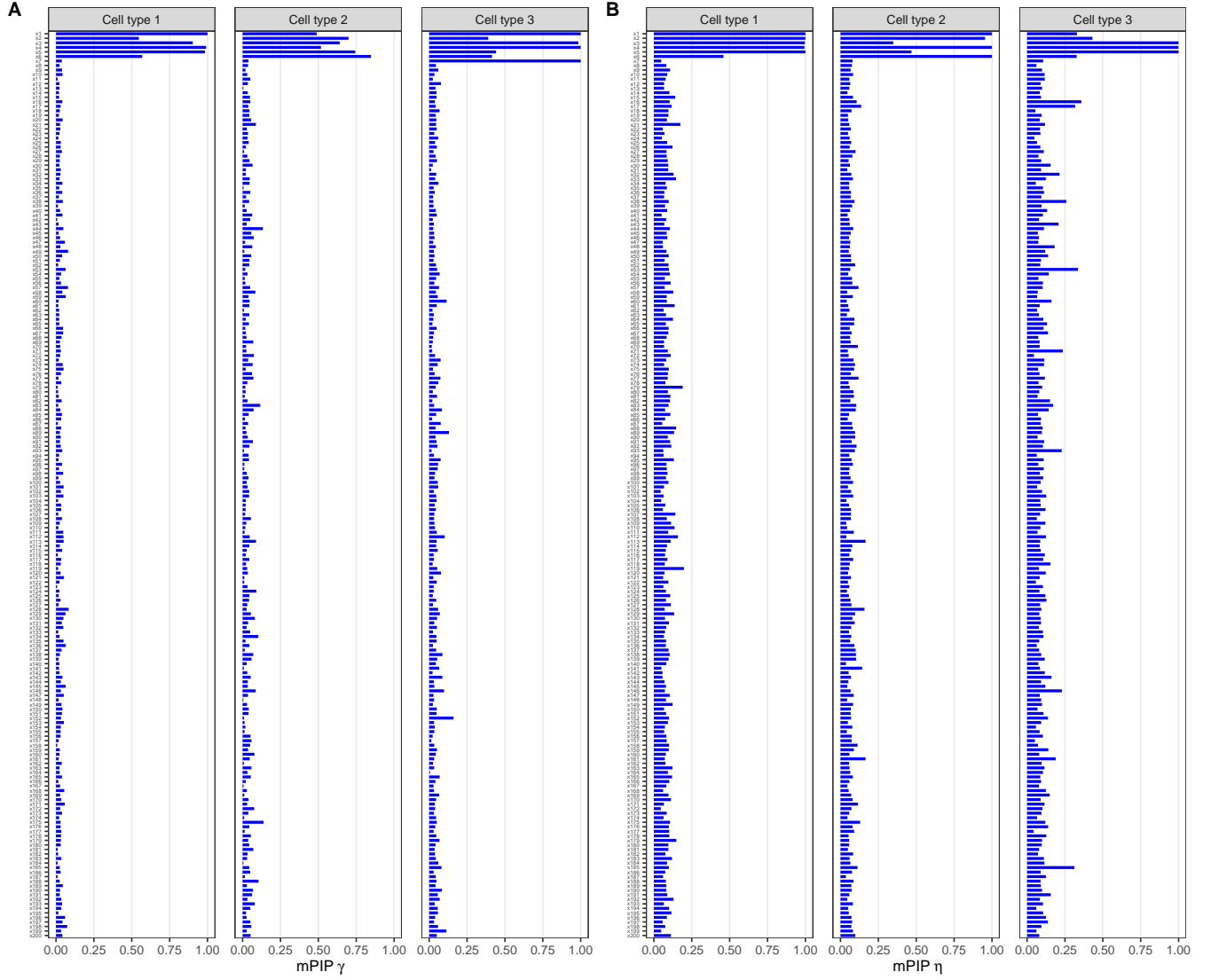


Figure 5: *Simulation results in high dimensions: Marginal posterior inclusion probabilities (mPIPs) of the variables linked to cell-type-specific survival and proportions by GPTCM-MRF2. (A) mPIPs of the variables linked to cell-type-specific survival. (B) mPIPs of the variables linked to cell-type-specific proportions.*



Table 3: Simulation results in high dimensions: Model estimation and variable selection

Model	$\frac{1}{\sqrt{pL}} \ \hat{\beta} - \beta\ _2$	$\frac{1}{\sqrt{pL}} \ \hat{\zeta} - \zeta\ _2$	Accuracy		Sensitivity		Specificity	
			$\gamma$	$\eta$	$\gamma$	$\eta$	$\gamma$	$\eta$
elastic net1	0.143		0.978		0.000		1.000	
elastic net2	0.146		0.968		0.154		0.986	
GPTCM-Ber1	0.103		0.988		0.462		1.000	
GPTCM-Ber2	0.089	0.022	0.992	1.000	0.615	1.000	1.000	1.000
GPTCM-MRF1	0.041		0.998		1.000		0.998	
GPTCM-MRF2	0.040	0.021	0.997	1.000	1.000	1.000	0.997	1.000

NOTE: The empty cells are due to no parameters in corresponding models. The variable selection of the GPTCMs is determined by the median probability model (MPM) with marginal posterior inclusion probability (mPIP) thresholded at 0.5. Note that the uncertainty for the estimation of the variable selection related parameters can be seen in Figure 5, Supplementary Figure S7, Supplementary Figure S8 and Supplementary Figure S3.

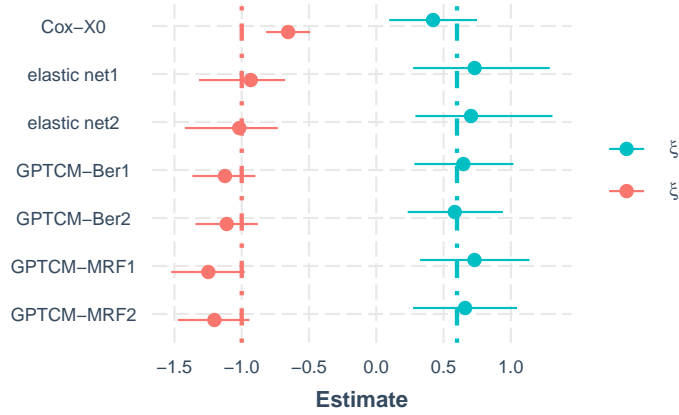


Figure 6: Simulation results in high dimensions: Estimates of the clinical variables' effects on the cure fraction. The circle point shows a point estimate (frequentist point estimate by Cox-X0, elastic net1 or elastic net2, or posterior mean by GPTCMs). The error bar shows a 95% confidence interval (by Cox-X0, elastic net1 or elastic net2) or a 95% credible interval (by GPTCMs). Note that the error bars of the two elastic net Cox models were estimated via the Bootstrapping. The green and red colored dot-dashed lines denote the true effects of the two clinical variables.

## 4 Discussion and conclusion

We have presented a class of six Bayesian versions of the generalized promotion time cure model (GPTCM) for both low-dimensional and high-dimensional data. The proposed Bayesian hierarchical modeling framework intuitively integrates multiscale data including individual level survival data, multicellular-level cell type proportions and cell-type-specific covariates. Four of the GTPCMs (i.e. GPTCM-Ber1, GPTCM-Ber2, GPTCM-MRF1 and GPTCM-MRF2) allows variable selection for cell-type-specific covariates, in which GPTCM-Ber2 and GPTCM-MRF2 allow variable selection for covariates linked to cell-type-specific survival and variable selection for covariates linked to cell-type-specific proportions. A unified full Bayesian inference has been provided for the computations of all the GPTCMs. In particular, the GPTCM with a MRF prior can make use of known biological network information between (cell-type-specific) covariates. When biological research advances, the GPTCM with a MRF prior could improve just from the improved network information provided, without any additional training data or improved methodology.

The simulation studies indicate that the GPTCMs with variable selection is useful when unrelated covariates are present in both low- and high-dimensional data for survival prognosis (Figures 1 and 4). Even if the model is misspecified with the data generating process by the Cox proportional hazards model with a few mandatory clinical variables, the GPTCMs with variable selection (i.e. GPTCM-Ber1, GPTCM-Ber2, GPTCM-MRF1 and GPTCM-MRF2) have slightly worse survival prognosis than the Cox model (Supplementary Figure S5), but the four GPTCMS can correctly identify unrelated covariates (Supplementary Figure S5), and GPTCM-MRF1 and GPTCM-MRF2 can also estimate the effects of the mandatory clinical variables as well as the Cox model (Supplementary Figure S6). Based on the prediction differences between the three GPTCMs with only modeling the cell-type-specific survival and the three GPTCMs with both modeling the cell-type-specific survival and proportions in both low and high dimensions (Figures 1 and 4), it was interesting to see that additionally modeling the proportions data can help for long-term survival prognosis, i.e. GPTCM-noBVS2, GPTCM-Ber2 and GPTCM-MRF2 outperform GPTCM-noBVS1, GPTCM-Ber1 and GPTCM-MRF1. This implies that tumor cell type proportions (together with cell-type-specific omics data) are useful for predicting cancer patient survival. If only using bulk sequencing omics data without distinguishing different cell types, it is difficult to identify cell-type-specific genes useful for guiding personalized treatment strategies to improve cancer patient survival.

In the simulations with high-dimensional covariates, both GPTCM-Ber2 and GPTCM-MRF2 identified truly related and truly unrelated covariates linked to the cell-type-specific proportions. This is might because the proportions are compositional data and the Dirichlet model is usually a good probabilistic model for compositional data. The GPTCM with a MRF prior can improve the identification of truly related cell-type-specific covariates if there is good prior knowledge for the biological network between omics variables.

There are several other possibilities for further work that could improve the proposed models. All the proposed Bayesian GPTCMs are parametric models. An alternative to the fully parametric settings is to use a semiparametric functional form instead of the parametric Weibull survival function for  $S_i(t)$  in GPTCM (1), which may improve the survival prediction under model misspecification as shown in Supplementary Figure S4 and remain good variable selection. Note that both the promotion time cure model (PTCM) and GPTCM are motivated by analyzing the mathematical dynamics of clonogenic tumor cells. However, the survival time or tumor growth should be also related to other types of cells, for example, immune cells. A more general and realistic model should account for the entire tumor microenvironment, for example, elucidating intercellular communication by modeling the interactions between tumor cell subtypes and immune cell subtypes and their omics information based on the data from single-cell RNA sequencing and spatial transcriptomics of

cancer tissues (Longo et al., 2021; Gulati et al., 2024). Also, the GPTCMs assume that the cell types are well categorized. But the discrete categorization based on single-cell RNA sequencing data tends to be an unsatisfactory model of the underlying biology (Ahlmann-Eltze and Huber, 2025), a latent embedding for cell-type categorization jointly with GPTCM can be for future improvements. Another limitation of the GPTCM modeling framework is that cell type proportions data are only from the diagnosis time of cancer patients. It would be ideal to obtain longitudinal information of the proportions data, which may more accurately model the tumor evolution and predict patient survival (Spitzer et al., 2025).

## Supplementary material

The supplementary materials contain the Bayesian posterior inference with full posterior conditional distributions and Metropolis-Hastings algorithms, and include additional simulation results. The R package **GPTCM** that implements all the proposed Bayesian GPTCMs is available in the GitHub repository <https://github.com/ocbe-uio/GPTCM>.

## Acknowledgments

This work was supported by the ERA PerMed under the ERA-NET Cofund scheme of the European Union’s Horizon 2020 research and innovation framework program (grant ‘SYMMETRY’ ERAPERMED2021-330).

## References

- Ahlmann-Eltze, C. and Huber, W. (2025). Analysis of multi-condition single-cell data with latent embedding multivariate regression. *Nature Genetics*, 57(3):659–667.
- Bender, R., Augustin, T., and Blettner, M. (2005). Generating survival times to simulate Cox proportional hazards models. *Statistics in Medicine*, 24(11):1713–1723.
- Cai, Y., Lu, Z., Chen, C., Zhu, Y., Chen, Z., Wu, Z., Peng, J., Zhu, X., Liu, Z., Li, B., Zhang, M., Huang, J., Li, Y., Liu, Y., Ma, Q., He, C., Chen, S., Tian, W., Fan, L., Ning, C., Geng, H., Xu, B., Li, H., Zhu, X., Fang, J., Wang, X., Zhang, S., Jin, M., Huang, C., Yang, X., Tian, J., and Miao, X. (2024). An atlas of genetic effects on cellular composition of the tumor microenvironment. *Nature Immunology*, 25(10):1959–1975.
- Chen, M.-H., Ibrahim, J. G., and Sinha, D. (1999). A new Bayesian model for survival data with a surviving fraction. *Journal of the American Statistical Association*, 94(447):909–919.
- Cooner, F., Banerjee, S., Carlin, B. P., and Sinha, D. (2007). Flexible cure rate modeling under latent activation schemes. *Journal of the American Statistical Association*, 102(478):560–572.
- Cox, D. R. (1972). Regression models and life-tables. *Journal of the Royal Statistical Society Series B: Statistical Methodology*, 34(2):187–202.
- Faucett, C. L. and Thomas, D. C. (1996). Simultaneously modelling censored survival data and repeatedly measured covariates: A Gibbs sampling approach. *Statistics in Medicine*, 15(15):1663–1685.

- Gilks, W. R., Best, N. G., and Tan, K. K. C. (1995). Adaptive rejection Metropolis sampling within Gibbs sampling. *Journal of the Royal Statistical Society Series C: Applied Statistics*, 44(4):455–472.
- Gulati, G. S., D’Silva, J. P., Liu, Y., Wang, L., and Newman, A. M. (2024). Profiling cell identity and tissue architecture with single-cell and spatial transcriptomics. *Nature Reviews Molecular Cell Biology*, 26(1):11–31.
- Gómez, Y. M., Gallardo, D. I., Bourguignon, M., Bertolli, E., and Calsavara, V. F. (2023). A general class of promotion time cure rate models with a new biological interpretation. *Lifetime Data Analysis*, 29(1):66–86.
- Kim, S., Chen, M.-H., and Dey, D. K. (2011). A new threshold regression model for survival data with a cure fraction. *Lifetime Data Analysis*, 17(1):101–122.
- Li, F. and Zhang, N. R. (2010). Bayesian variable selection in structured high-dimensional covariate spaces with applications in genomics. *Journal of the American Statistical Association*, 105(491):1202–1214.
- Longo, S. K., Guo, M. G., Ji, A. L., and Khavari, P. A. (2021). Integrating single-cell and spatial transcriptomics to elucidate intercellular tissue dynamics. *Nature Reviews Genetics*, 22(10):627–644.
- Ma, Y. and Yin, G. (2008). Cure rate model with mismeasured covariates under transformation. *Journal of the American Statistical Association*, 103(482):743–756.
- Maier, M. J. (2014). DirichletReg: Dirichlet regression for compositional data in R. Research Report Series/Department of Statistics and Mathematics 125, WU Vienna University of Economics and Business, Vienna.
- Neal, R. M. (2003). Slice sampling. *The Annals of Statistics*, 31(3):705–767.
- Simon, N., Friedman, J., Hastie, T., and Tibshirani, R. (2011). Regularization paths for Cox’s proportional hazards model via coordinate descent. *Journal of Statistical Software*, 39(5):1–13.
- Spitzer, A., Johnson, K. C., Nomura, M., Garofano, L., Nehar-belaid, D., Darnell, N. G., Greenwald, A. C., Bussema, L., Oh, Y. T., Varn, F. S., D’Angelo, F., Gritsch, S., Anderson, K. J., Migliozi, S., Gonzalez Castro, L. N., Chowdhury, T., Robine, N., Reeves, C., Park, J. B., Lipsa, A., Hertel, F., Golebiewska, A., Niclou, S. P., Nusrat, L., Kellet, S., Das, S., Moon, H.-E., Paek, S. H., Bielle, F., Laurence, A., Di Stefano, A. L., Mathon, B., Picca, A., Sanson, M., Tanaka, S., Saito, N., Ashley, D. M., Keir, S. T., Ligon, K. L., Huse, J. T., Yung, W. K. A., Lasorella, A., Iavarone, A., Verhaak, R. G. W., Tirosh, I., and Suvà, M. L. (2025). Deciphering the longitudinal trajectories of glioblastoma ecosystems by integrative single-cell genomics. *Nature Genetics*, 57(5):1168–1178.
- Stingo, F. C., Chen, Y. A., Tadesse, M. G., and Vannucci, M. (2011). Incorporating biological information into linear models: A Bayesian approach to the selection of pathways and genes. *The Annals of Applied Statistics*, 5(3):1978–2002.
- Thompson, W. R. (1933). On the likelihood that one unknown probability exceeds another in view of the evidence of two samples. *Biometrika*, 25(3–4):285–294.
- Vehtari, A., Simpson, D., Gelman, A., Yao, Y., and Gabry, J. (2024). Pareto smoothed importance sampling. *Journal of Machine Learning Research*, 25:1–58.

- Yakovlev, A. Y., Tsodikov, A. D., and Asselain, B. (1996). *Stochastic Models of Tumor Latency and Their Biostatistical Applications*. World Scientific, Singapore.
- Zhang, A., Miao, K., Sun, H., and Deng, C.-X. (2022). Tumor heterogeneity reshapes the tumor microenvironment to influence drug resistance. *International Journal of Biological Sciences*, 18(7):3019–3033.
- Zhao, Z., Banterle, M., Lewin, A., and Zucknick, M. (2024a). Multivariate Bayesian structured variable selection for pharmacogenomic studies. *Journal of the Royal Statistical Society Series C: Applied Statistics*, 73(2):420–443.
- Zhao, Z. and Kızılaslan, F. (2024). A note on promotion time cure models with a new biological consideration. arXiv:2408.17188.
- Zhao, Z., Zolas, J., Zucknick, M., and Aittokallio, T. (2024b). Tutorial on survival modeling with applications to omics data. *Bioinformatics*, 40(3):btac132.

Supplementary materials for  
 “Generalized promotion time cure model: A new modeling frame-  
 work to identify cell-type-specific genes and improve survival prog-  
 nosis”

## S1 Posterior inference

The joint posterior distribution is composed by the likelihood and the joint prior, see Section 2.3. Based on that, all available full posterior conditional distributions are as follows.

$$\begin{aligned}
 f(\beta_{jl} | \gamma_{jl} = 1, \text{---}) &\propto \prod_{i=1}^n \left\{ e^{-\theta_i(1-\sum_{l'} \mathbf{p}_{il'} e^{-(t_i/\lambda_{il'})^\kappa})} \theta_i \kappa t_i^{\kappa-1} \sum_{l'} \mathbf{p}_{il'} \lambda_{il'}^{-\kappa} e^{-(t_i/\lambda_{il'})^\kappa} \right\}^{\delta_i} \\
 &\quad \times \left\{ e^{-\theta_i(1-\sum_{l'} \mathbf{p}_{il'} e^{-(t_i/\lambda_{il'})^\kappa})} \right\}^{1-\delta_i} \times e^{-\frac{\beta_{jl}^2}{2\tau_l^2}} \\
 &\propto \prod_{i=1}^n \left\{ \sum_{l'} \frac{\kappa}{\lambda_{il'}} \left( \frac{t_i}{\lambda_{il'}} \right)^{\kappa-1} \mathbf{p}_{il'} e^{-(t_i/\lambda_{il'})^\kappa} \right\}^{\delta_i} e^{\theta_i \mathbf{p}_{il} e^{-(t_i/\lambda_{il})^\kappa} - \frac{\beta_{jl}^2}{2\tau_l^2}}, \quad j = 1, \dots, p, \quad l = 1, \dots, L,
 \end{aligned}$$

where  $\log \lambda_{il} = \frac{\mu_{il}}{\Gamma(1+1/\kappa)}$ ,  $\mu_{il} = \beta_{0l} + \mathbf{X}_{il} \boldsymbol{\beta}_l$ . Note that the conditional part with notation “—” means all relevant parameters. If  $\gamma_{jl} = 0$ , then  $\beta_{jl} = 0$  without the need of a posterior conditional distribution.

$$\begin{aligned}
 f(\beta_{0l} | \text{---}) &\propto \prod_{i=1}^n \left\{ e^{-\theta_i(1-\sum_{l'} \mathbf{p}_{il'} e^{-(t_i/\lambda_{il'})^\kappa})} \theta_i \kappa t_i^{\kappa-1} \sum_{l'} \mathbf{p}_{il'} \lambda_{il'}^{-\kappa} e^{-(t_i/\lambda_{il'})^\kappa} \right\}^{\delta_i} \\
 &\quad \times \left\{ e^{-\theta_i(1-\sum_{l'} \mathbf{p}_{il'} e^{-(t_i/\lambda_{il'})^\kappa})} \right\}^{1-\delta_i} \times e^{-\frac{\beta_{0l}^2}{2\tau_0^2}} \\
 &\propto \prod_{i=1}^n \left\{ \sum_{l'} \frac{\kappa}{\lambda_{il'}} \left( \frac{t_i}{\lambda_{il'}} \right)^{\kappa-1} \mathbf{p}_{il'} e^{-(t_i/\lambda_{il'})^\kappa} \right\}^{\delta_i} e^{\theta_i \mathbf{p}_{il} e^{-(t_i/\lambda_{il})^\kappa} - \frac{\beta_{0l}^2}{2\tau_0^2}}, \quad j = 1, \dots, p, \quad l = 1, \dots, L.
 \end{aligned}$$

$$f(\pi_{jl} | \text{---}) \propto \prod_{l'=1}^L \prod_{j'=1}^p f(\gamma_{j'l'} | \pi_{j'l'}) \cdot \text{Beta}(a_\pi, b_\pi) \sim \text{Beta}(a_\pi + \gamma_{jl}, b_\pi + p - \gamma_{jl})$$

$$f(\tau_l^2 | \text{---}) \propto \prod_{l'=1}^L \prod_{j=1}^p f(\beta_{jl'} | \gamma_{jl'} = 1, \tau_{l'}^2) \cdot \text{IGamma}(a_\tau, b_\tau) \sim \text{IGamma} \left( a_\tau + 0.5 \sum_j \gamma_{jl}, b_\tau + 0.5 \sum_j \beta_{jl}^2 \right)$$

$$\begin{aligned}
 f(\xi_j | \text{---}) &\propto \prod_{i=1}^n \left\{ e^{-\theta_i(1-\sum_l \mathbf{p}_{il} S_l(t_i))} \theta_i \kappa t_i^{\kappa-1} \sum_l \mathbf{p}_{il} \lambda_{il}^{-\kappa} S_l(t_i) \right\}^{\delta_i} \left\{ e^{-\theta_i(1-\sum_l \mathbf{p}_{il} S_l(t_i))} \right\}^{1-\delta_i} e^{-\frac{\xi_j^2}{2v_j^2}} \\
 &\propto \prod_{i=1}^n \theta_i^{\delta_i} e^{-\theta_i(1-\sum_l \mathbf{p}_{il} S_l(t_i)) - \frac{\xi_j^2}{2v_j^2}}, \quad \text{where } \theta_i = \exp\{\xi_0 + \mathbf{X}_{0i} \boldsymbol{\xi}\}, \quad \boldsymbol{\xi} = [\xi_1, \dots, \xi_d]^\top, \quad j = 1, \dots, d
 \end{aligned}$$

$$f(\xi_0 | \text{---}) \propto \prod_{i=1}^n \theta_i^{\delta_i} e^{-\theta_i(1-\sum_l \mathbf{p}_{il} S_l(t_i)) - \frac{\xi_0^2}{2v_0^2}}, \text{ where } \theta_i = \exp\{\xi_0 + \mathbf{X}_{0i}\boldsymbol{\xi}\}$$

$$f(v_j^2 | \text{---}) \propto \prod_{j'=1}^d f(\xi_{j'} | v_{j'}^2) \cdot \mathcal{IGamma}(a_v, b_w) \sim \mathcal{IGamma}\left(a_v + 1, b_w + 0.5 \sum_{j'} \xi_{j'}^2\right)$$

$$\begin{aligned} f(\kappa | \text{---}) &\propto \prod_{i=1}^n \left\{ e^{-\theta_i(1-\sum_l \mathbf{p}_{il} S_l(t_i))} \theta_i \kappa t_i^{\kappa-1} \sum_l \mathbf{p}_{il} \lambda_{il}^{-\kappa} S_l(t_i) \right\}^{\delta_i} \left\{ e^{-\theta_i(1-\sum_l \mathbf{p}_{il} S_l(t_i))} \right\}^{1-\delta_i} \cdot \mathcal{Gamma}(a_\kappa, b_\kappa) \\ &\propto \prod_{i=1}^n \left\{ \sum_l \frac{\kappa}{\lambda_{il}} \left( \frac{t_i}{\lambda_{il}} \right)^{\kappa-1} \mathbf{p}_{il} S_l(t_i) \right\}^{\delta_i} e^{\theta_i \sum_l \mathbf{p}_{il} S_l(t_i)} \cdot \mathcal{Gamma}(a_\kappa, b_\kappa) \end{aligned}$$

$$\begin{aligned} f(\zeta_{jl} | \eta_{jl} = 1, \text{---}) &\propto \prod_{i=1}^n \left\{ e^{-\theta_i(1-\sum_{l'} \mathbf{p}_{il'} S_{l'}(t_i))} \theta_i \kappa t_i^{\kappa-1} \sum_{l'} \mathbf{p}_{il'} \lambda_{il'}^{-\kappa} S_{l'}(t_i) \right\}^{\delta_i} \left\{ e^{-\theta_i(1-\sum_{l'} \mathbf{p}_{il'} S_{l'}(t_i))} \right\}^{1-\delta_i} \\ &\quad \cdot f(\tilde{\mathbf{p}}_i | \mathbf{p}_i, \phi) \prod_{l'=1}^L \prod_{j'=1}^p f(\zeta_{j'l'} | \eta_{j'l'} = 1, \rho_{j'l'}) \\ &\propto \prod_{i=1}^n \left\{ \sum_{l'} \frac{\kappa}{\lambda_{il'}} \left( \frac{t_i}{\lambda_{il'}} \right)^{\kappa-1} \mathbf{p}_{il'} S_{l'}(t_i) \right\}^{\delta_i} e^{\theta_i \sum_{l'} \mathbf{p}_{il'} S_{l'}(t_i)} \cdot \frac{\Gamma(\alpha_{i0})}{\prod_{l'} \Gamma(\alpha_{il'})} \prod_{l'} \tilde{\mathbf{p}}_{il'}^{\alpha_{il'}-1} \cdot e^{-\frac{\zeta_{jl}^2}{2w_l^2}} \\ &\propto \prod_{i=1}^n \left\{ \sum_{l'} \lambda_{il'}^{-\kappa} \frac{\alpha_{il'}}{\alpha_{i0}} S_{l'}(t_i) \right\}^{\delta_i} e^{\theta_i \sum_{l'} \frac{\alpha_{il'}}{\alpha_{i0}} S_{l'}(t_i)} \cdot \frac{\Gamma(\alpha_{i0})}{\prod_{l'} \Gamma(\alpha_{il'})} \prod_{l'} \tilde{\mathbf{p}}_{il'}^{\alpha_{il'}-1} \cdot e^{-\frac{\zeta_{jl}^2}{2w_l^2}} \end{aligned}$$

$$f(\zeta_{0l} | \text{---}) \propto \prod_{i=1}^n \left\{ \sum_{l'} \lambda_{il'}^{-\kappa} \frac{\alpha_{il'}}{\alpha_{i0}} \mathbf{p}_{il'} S_{l'}(t_i) \right\}^{\delta_i} e^{\theta_i \sum_{l'} \frac{\alpha_{il'}}{\alpha_{i0}} S_{l'}(t_i)} \cdot \frac{\Gamma(\alpha_{i0})}{\prod_{l'} \Gamma(\alpha_{il'})} \prod_{l'} \tilde{\mathbf{p}}_{il'}^{\alpha_{il'}-1} \cdot e^{-\frac{\zeta_{0l}^2}{2w_0^2}}$$

$$f(\rho_{jl} | \text{---}) \propto \prod_{l'=1}^L \prod_{j'=1}^p f(\eta_{j'l'} | \rho_{j'l'}) \cdot \mathcal{Beta}(a_\rho, b_\rho) \sim \mathcal{Beta}(a_\rho + \eta_{jl}, b_\rho + p - \eta_{jl})$$

$$f(w_l^2 | \text{---}) \propto \prod_{l'=1}^L \prod_{j=1}^p f(\zeta_{jl'} | \eta_{jl'} = 1, w_{l'}^2) \cdot \mathcal{IGamma}(a_w, b_w) \sim \mathcal{IGamma}\left(a_w + 0.5 \sum_j \eta_{jl}, b_w + 0.5 \sum_j \zeta_{jl}^2\right)$$

$$f(w_0^2 | \text{---}) \propto \prod_{l=1}^L f(\zeta_{0l} | w_0^2) \cdot \mathcal{IGamma}(a_{w_0}, b_{w_0}) \sim \mathcal{IGamma}\left(a_{w_0} + 0.5L, b_{w_0} + 0.5 \sum_l \zeta_{0l}^2\right)$$

- **$\gamma$  sampling**

For a randomly chosen  $l$ -th cell type, we use the Metropolis-Hastings algorithm to update  $\gamma_l$  with acceptance probability

$$\min \left\{ 1, \frac{f(\gamma_l^*)f(\mathcal{D}|\gamma_l^*, \beta_l^*, \text{---})}{f(\gamma_l)f(\mathcal{D}|\gamma_l, \beta_l, \text{---})} \times \frac{q(\gamma_l|\gamma_l^*)}{q(\gamma_l^*|\gamma_l)} \right\},$$

where  $\gamma_l^*$  is the proposed indicator variables and  $\beta_l^*$  is the proposed coefficients based on  $\gamma_l^*$ . With the MC3 sampling, we use symmetric proposal distribution  $q_{\gamma_l}(\gamma_l|\gamma_l^*) = q_{\gamma_l}(\gamma_l^*|\gamma_l) \sim \text{Bernoulli}(0.5)$ . With the Thompson sampling by using multi-armed bandit algorithm, we will evaluate all previous Bayesian variable selection in the proposal ratio  $q(\gamma_l|\gamma_l^*)/q(\gamma_l^*|\gamma_l)$ .

- **$\eta$  sampling**

Using the same approach as  $\gamma$  sampling.



## S2 Additional simulation results in low dimensions

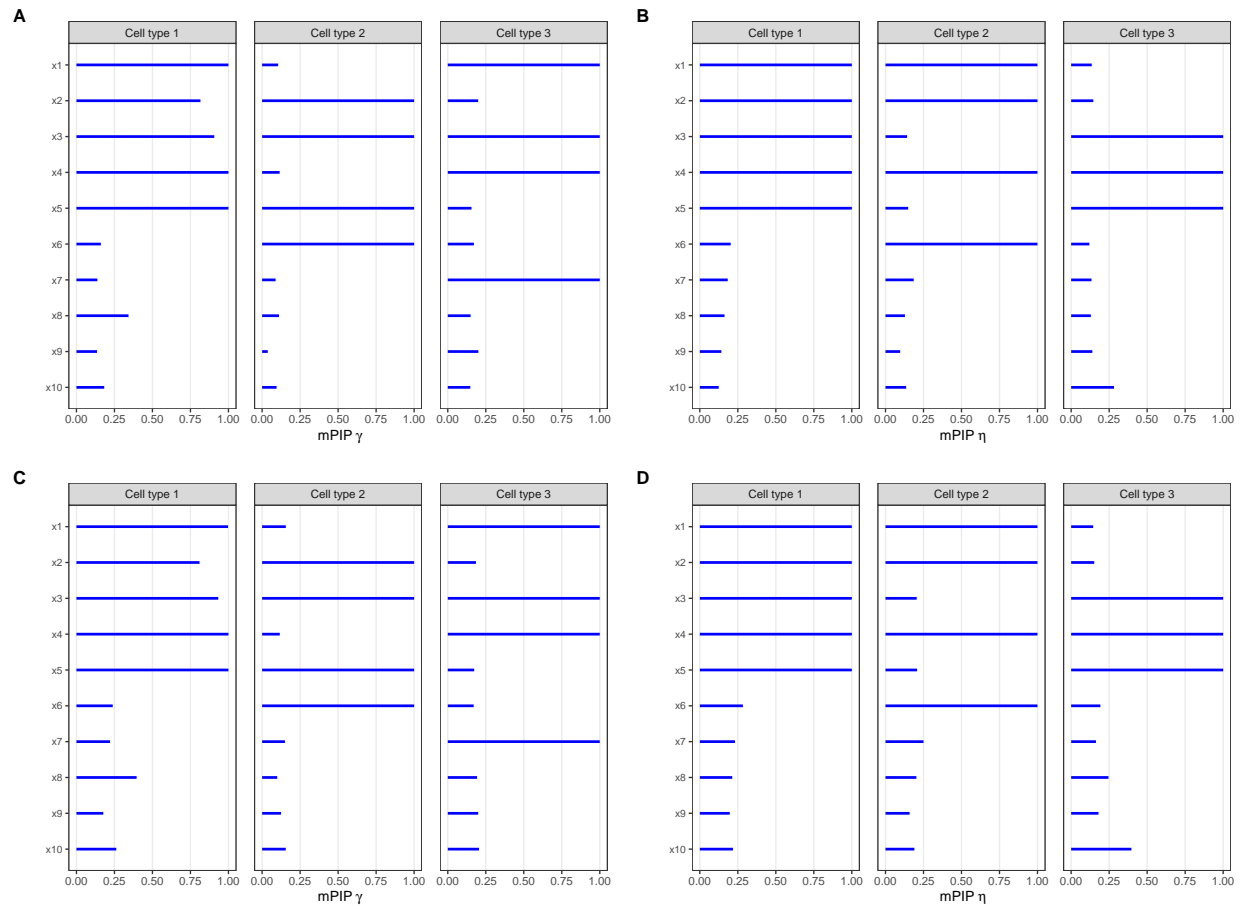


Figure S1: *Simulation results in low dimensions: Marginal posterior inclusion probabilities (mPIPs) of the variables linked to cell-type-specific survival and proportions by GPTCM-MRF2 and GPTCM-Ber2. (A) mPIPs of the variables linked to cell-type-specific survival by GPTCM-MRF2. (B) mPIPs of the variables linked to cell-type-specific proportions by GPTCM-MRF2. (C) mPIPs of the variables linked to cell-type-specific survival by GPTCM-Ber2. (D) mPIPs of the variables linked to cell-type-specific proportions by GPTCM-Ber2.*

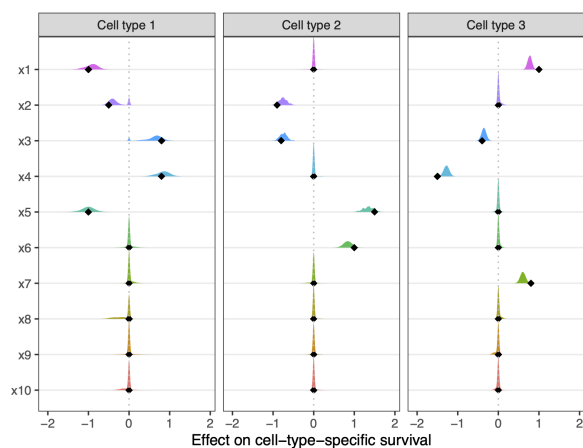
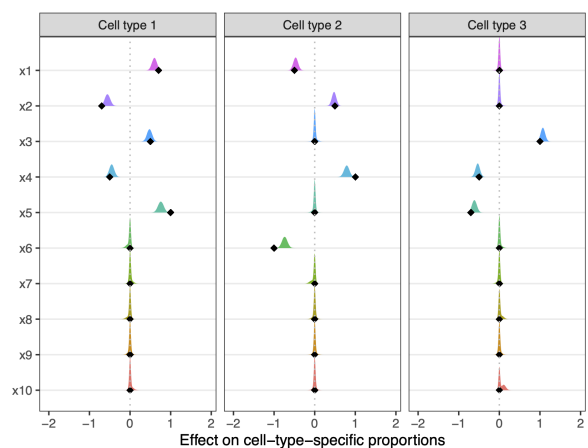
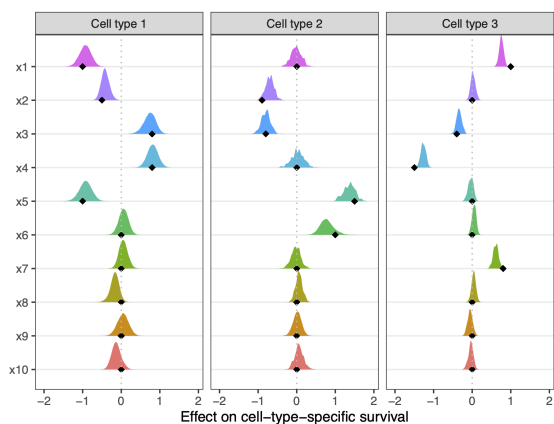
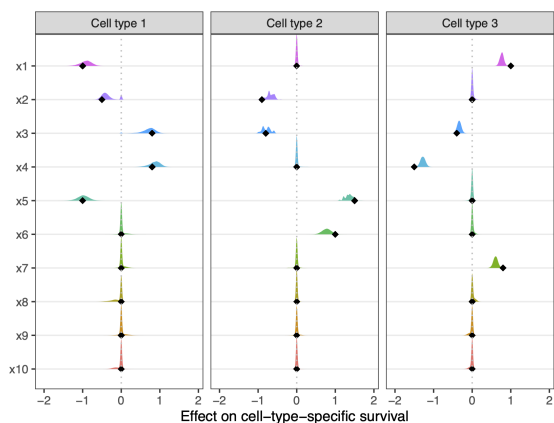
**A****B**

Figure S2: *Simulation results in low dimensions: Posterior distributions of the effects on cell-type-specific survival and proportions by GPTCM-Ber2. The black colored diamond indicates the true effect. (A) Posterior distributions of the effects on cell-type-specific survival. (B) Posterior distributions of the effects on cell-type-specific proportions by the GPTCM-noBVS2.*

**A**



**B**



**C**

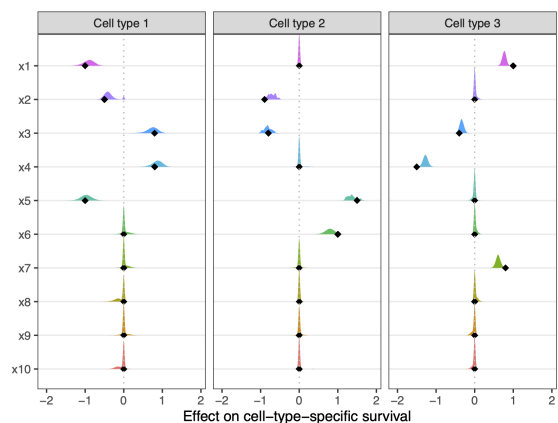


Figure S3: *Simulation results in low dimensions: Posterior distributions of the effects on cell-type-specific survival. The black colored diamond indicates the true effect. (A) Posterior distributions of the effects on cell-type-specific survival by GPTCM-noBVS1. (B) Posterior distributions of the effects on cell-type-specific survival by GPTCM-Ber1. (C) Posterior distributions of the effects on cell-type-specific proportions by GPTCM-MRF1.*

### S3 Simulation results in low dimensions for assessing model misspecification

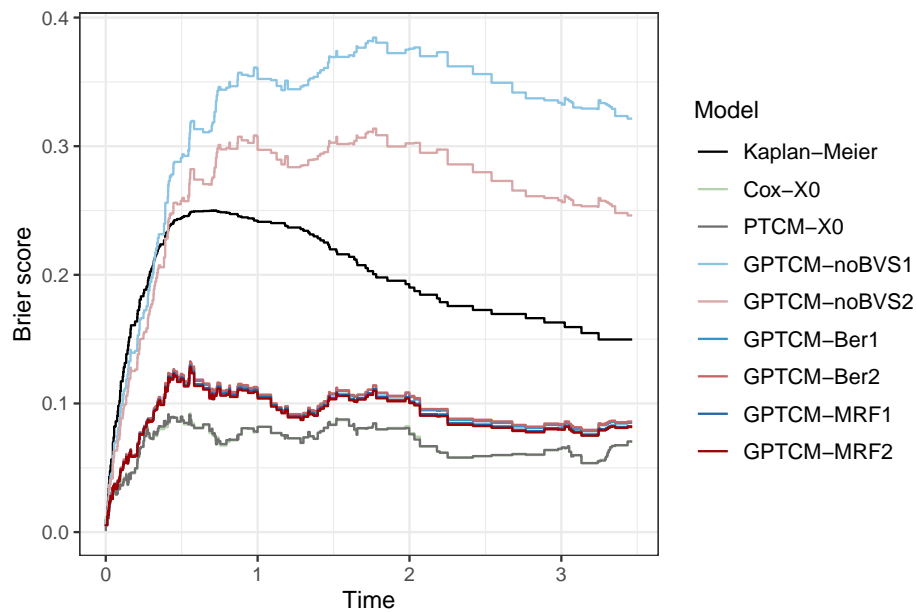


Figure S4: *Simulation results in low dimensions under model misspecification: Prediction errors of classical survival models and GPTCMs in terms of time-dependent Brier score. The Kaplan-Meier method is as a reference that did not account for any covariate. The predictions of GPTCM-noBVS1 and GPTCM-noBVS2 were based on the posterior mean of all parameters. The predictions of other GPTCMs were based on the estimates of their median probability models (MPMs) for the effects of covariates with variable selection and estimates of posterior mean for other parameters.*

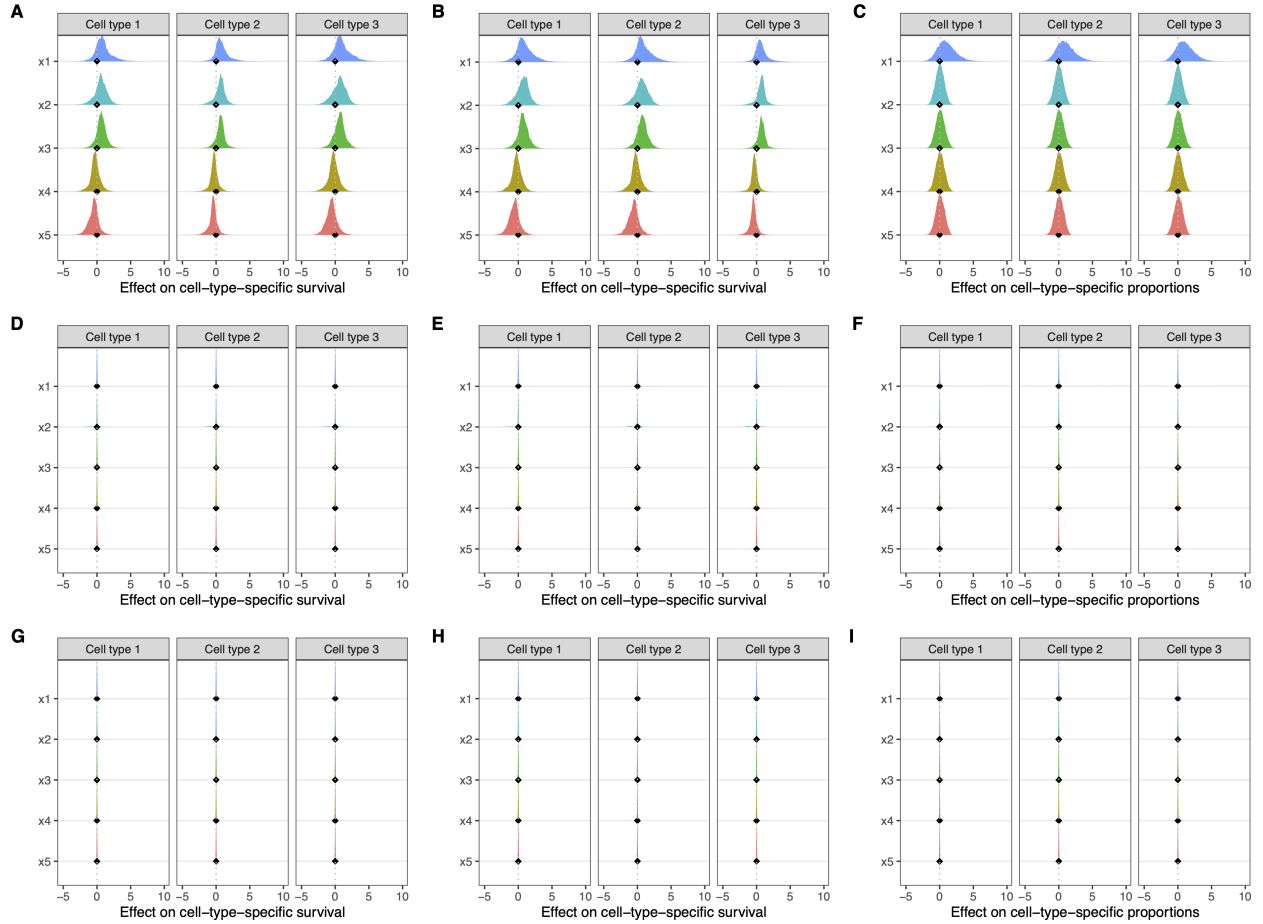


Figure S5: *Simulation results in low dimensions under model misspecification: Posterior distributions of the effects on cell-type-specific survival and on cell-type-specific proportions. The black colored diamond indicates the true effect. (A) Posterior distributions of the effects on cell-type-specific survival by GPTCM-noBVS1. (B) Posterior distributions of the effects on cell-type-specific survival by GPTCM-noBVS2. (C) Posterior distributions of the effects on cell-type-specific proportions by GPTCM-noBVS2. (D) Posterior distributions of the effects on cell-type-specific survival by GPTCM-Ber1. (E) Posterior distributions of the effects on cell-type-specific survival by GPTCM-Ber2. (F) Posterior distributions of the effects on cell-type-specific proportions by GPTCM-Ber2. (G) Posterior distributions of the effects on cell-type-specific survival by GPTCM-MRF1. (H) Posterior distributions of the effects on cell-type-specific survival by GPTCM-MRF2. (I) Posterior distributions of the effects on cell-type-specific proportions by GPTCM-MRF2.*

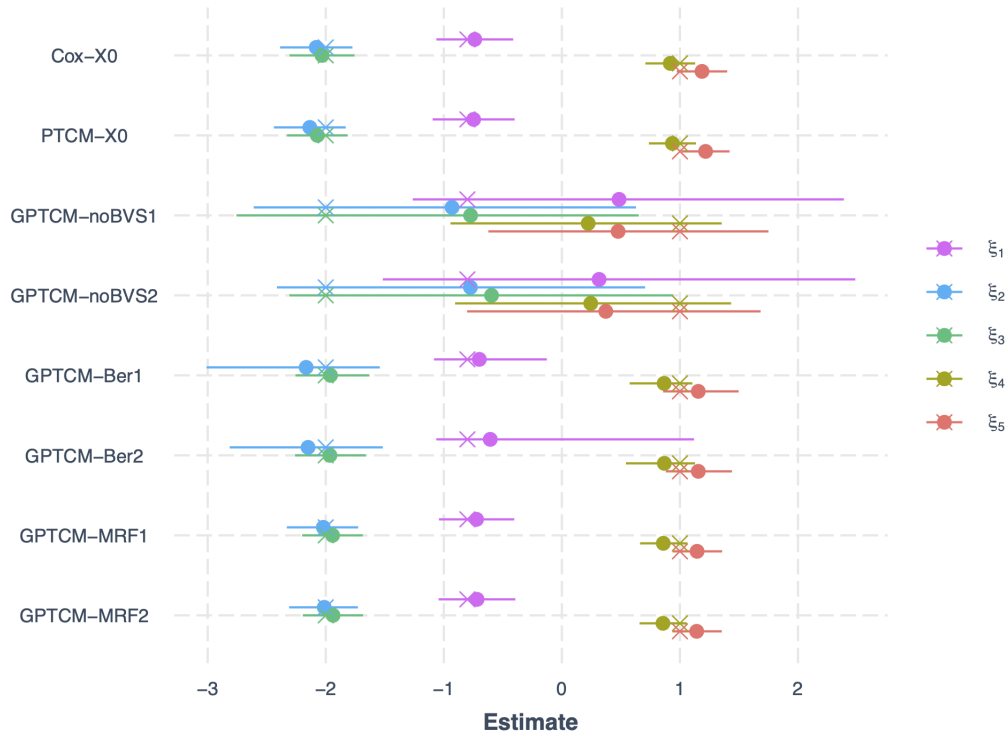


Figure S6: *Simulation results in low dimensions under model misspecification: Estimates of the clinical variables' effects on the cured fraction. The circle point shows a point estimate (posterior mean if it corresponds to a Bayesian GPTCM). The error bar shows a 95% confidence or credible interval. The cross shape denotes the true effect of a clinical variable.*

## S4 Additional simulation results in high dimensions

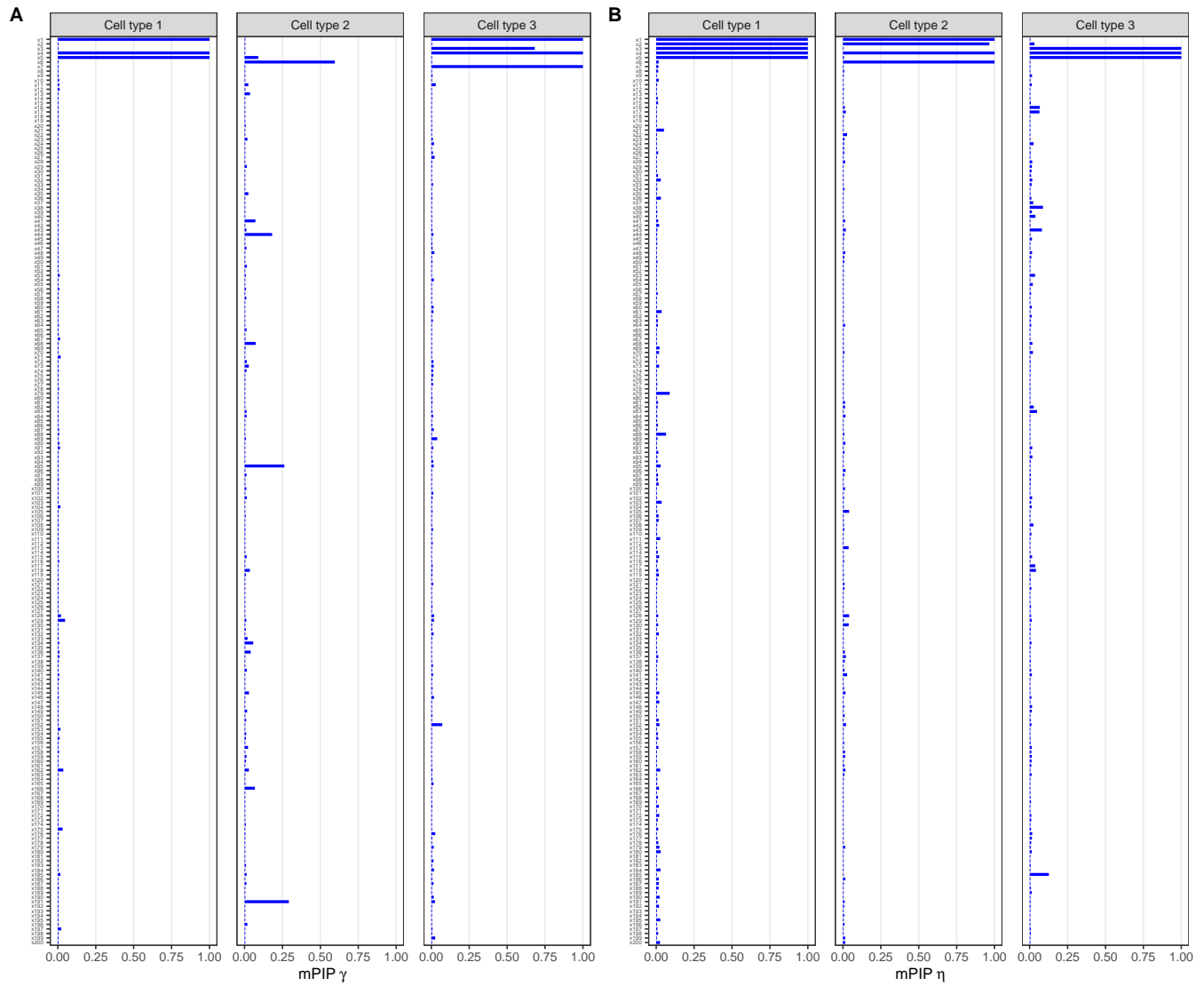


Figure S7: *Simulation results in high dimensions: Marginal posterior inclusion probabilities (mPIPs) of the variables linked to cell-type-specific survival and proportions by GPTCM-Ber2. (A) mPIPs of the variables linked to cell-type-specific survival. (B) mPIPs of the variables linked to cell-type-specific proportions.*

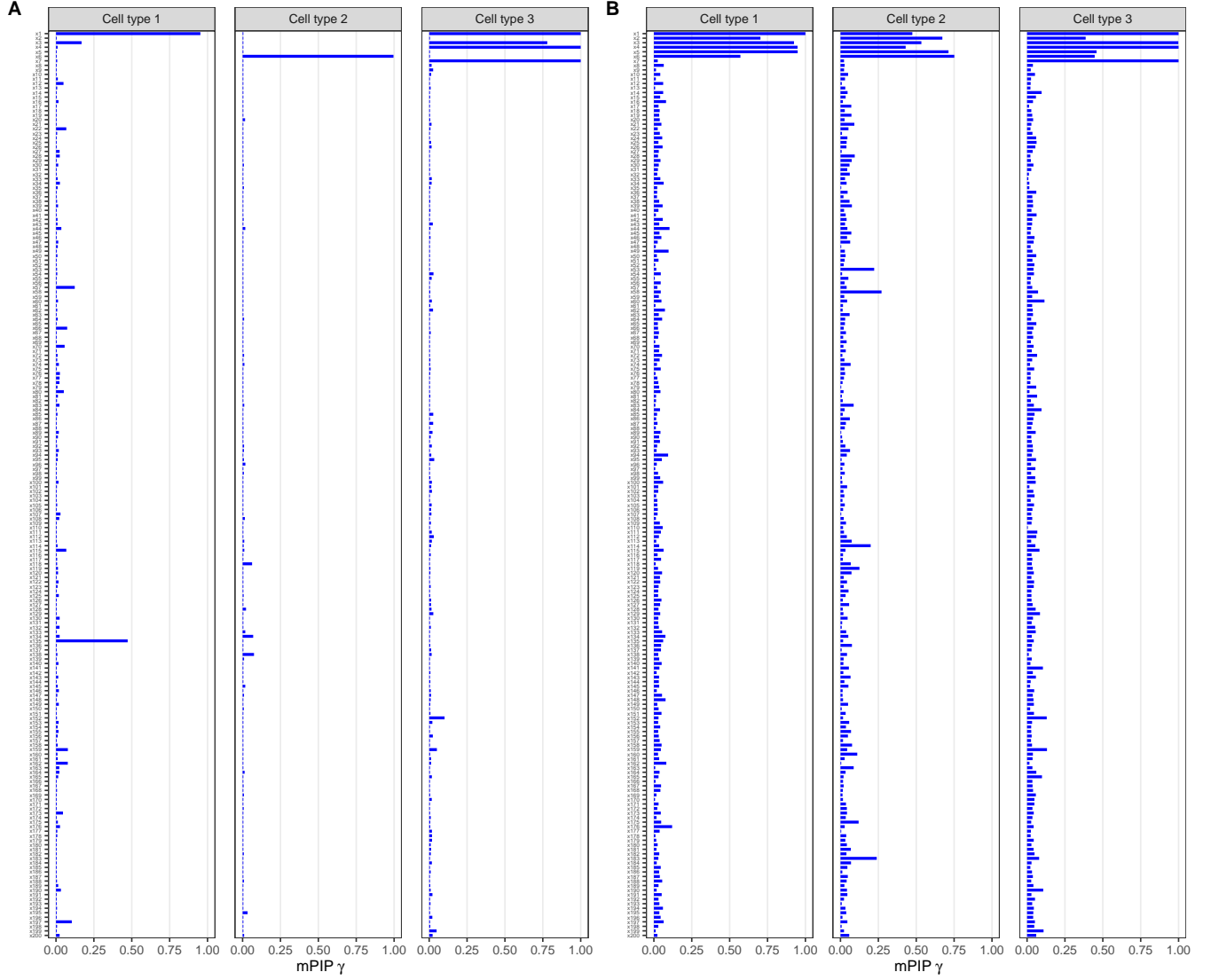


Figure S8: *Simulation results in high dimensions: Marginal posterior inclusion probabilities (mPIPs) of the variables linked to cell-type-specific survival and proportions by GPTCM-Ber1 and GPTCM-MRF1. (A) mPIPs of the variables linked to cell-type-specific survival by GPTCM-Ber1. (B) mPIPs of the variables linked to cell-type-specific survival by GPTCM-MRF1.*



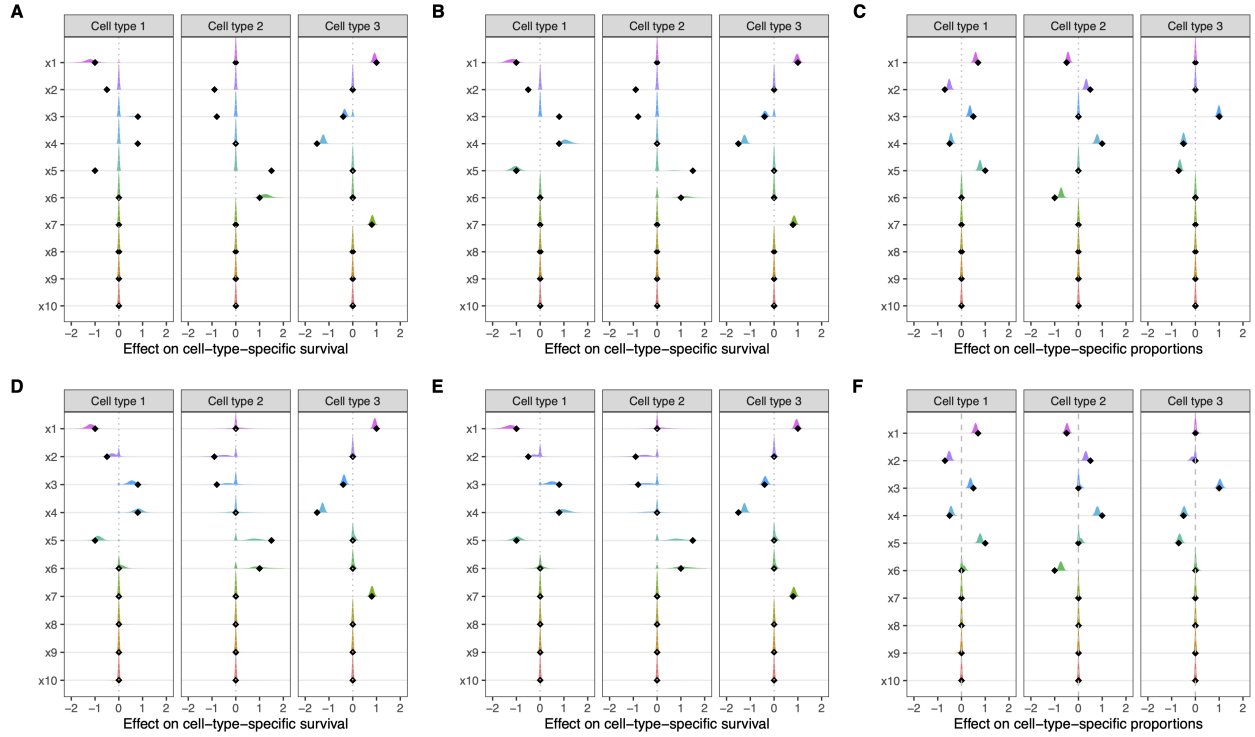


Figure S9: *Simulation results in high dimensions: The first 10 posterior distributions of the effects on cell-type-specific survival and proportions by GPTCM-Ber1, GPTCM-Ber2, GPTCM-MRF1, and GPTCM-MRF2. The black colored diamond indicates the true effect. (A) Posterior distributions of the effects on cell-type-specific survival by GPTCM-Ber1. (B) Posterior distributions of the effects on cell-type-specific survival by GPTCM-Ber2. (C) Posterior distributions of the effects on cell-type-specific proportions by GPTCM-Ber2. (D) Posterior distributions of the effects on cell-type-specific survival by GPTCM-MRF1. (E) Posterior distributions of the effects on cell-type-specific survival by GPTCM-MRF2. (F) Posterior distributions of the effects on cell-type-specific proportions by GPTCM-MRF2.*